Review

Removal of Hazardous Organic Dyes from Liquid Wastes Using Advanced Nanomaterials

Francisco Jose Alguacil * and Manuel Alonso

Posted Date: 17 May 2024

doi: 10.20944/preprints202405.1122.v1

Keywords: nanomaterials; organic dyes; removal; environment

Review

Removal of Hazardous Organic Dyes from Liquid Wastes Using Advanced Nanomaterials

Francisco Jose Alguacil * and Manuel Alonso

Centro Nacional de Investigaciones Metalurgicas (CSIC). Avda. Gregorio del Amo 8. 28040 Madrid. Spain
* Correspondence: fjalgua@cenim.csic.es

Abstract: The presence of organic dyes in aqueous environments is of extreme hazardousness against life due to the toxicity of these compounds. Thus, its removal from these various aquatic media is of the utmost importance and several technologies are constantly proven to match this goal. Among these technologies, various types of degradation and adsorption are the most widely used, and of the various types of materials used within these technologies, nanomaterials are constantly developed and investigated, probably due to the various properties that these nanomaterials presented. This work reviewed recent developments (2023 year) about the use of these nanomaterials on the treatment of solutions contaminated with these toxic organic dyes.

Keywords: nanomaterials; organic dyes; removal; environment

1. Introduction

Organic dyes are commonly used chemicals in textile industry to give colour to the various products manufactured in it. As consequence of this use, the effluents produced within this industry contained variable concentrations of these harmful dyes, thus its removal from these effluents is of the utmost necessity to avoid environmental issues.

To remove these dyes, many type of materials are using, and among them, nanomaterials are gaining a considerable importance due to its inherent properties. The importance of the removal of these dyes and the use of nanomaterials on this removal it reflects in the number or recent reviews about this matter. Table 1 summarized the different classes of nanomaterials recently reviewed (2023 year), as it can be seen there is an amply subclasses of this type of materials, and the way in which they remove organic dyes from the effluents is mainly by two type of processes: adsorption and/or (photo)catalysis.

The present work reviewed the most recent literature (papers published in 2023 year) about this field of interest as the use of nanomaterials in the removal or organic dyes is; this review classified the investigation considering the type of dyes involved in the literature: anionic, cationic and nanomaterials used for the treatment of both anionic and cationic dyes.

Table 1. Some recent reviews about the use of nanomaterials on the removal of organic dyes from solutions.

Nanomaterial	Reference
Heteropolyacids-supported on nanocatalysts	[1]
Nanomaterials	[2–8]
Bi-based nanocompounds	[9–11]
Graphitic carbon nitride	[12,13]
Sr-based nanomaterials	[14]
Nano-metal oxides-activated carbon	[15]

 doi:10.20944/preprints202405.1122.v1

TiO_2-based nanomaterials	[16–19]
Nanoparticle-hybridized polyaniline	[20]
Metal ferrites-based nanomaterials	[21]
Metal sulphides-based nanostructures	[22,23]
Polymeric nanocomposite membranes	[24,25]
Metals and metals oxides in pure form	[26–30]
Graphene-based nanomaterials	[31,32]
Cellulose-based nanocompounds	[33–35]
Biomass-metallic nanoparticles	[36]
Nanozymes	[37–40]
2D MXene-based adsorbents	[41–43]
Ba-TiO_3 nanomaterials	[44]
Gum-based nanomaterials	[45]
Chitosan-based nanomaterials	[46]
Carbon-based nanomaterials	[47,48]

2. Nanomaterials and Anionic Organic Dyes

2.1. Adsorption of Anionic Dyes on Nanomaterials

Computational investigation was used to study the performance of TiO_2 in the uptake of Acid Yellow 36 and Acid Orange 6 dyes on (1 1 0) surface of the oxide [49] . The results of these simulations indicated that Acid Yellow 36 was more reactive and had a greater adsorption uptake than Acid Orange 6.

Gelatin-bearing semi-IPN hydrogels containing different concentrations of itaconic acid-based protic ionic liquids (PILs) were prepared to remove Reactive Red 21 and Reactive Blue 19 from water [50]. When the hydrogels contained zero or low PILs concentrations, the adsorption uptake was maximum, being the best-performing hydrogel composition (GelITA1) tested in real wastewater (cotton samples were dyed with both dyes and the resulted wastewater was used in the experimentation) with an average 75% removal efficiency of the dyes. Maximum dye uptakes were 106 mg/g and 147 mg/g for Reactive Red 21 and Reactive Blue 19, respectively.

ZnO/C nanocomposites were fabricated at temperatures in the 500-700º C range. Among all the composites, ZnO/C-700 sample was the nanomaterial with better adsorption characteristics for the removal of Congo Red from solutions [51]. The maximum ye load was near 47 mg/g

Sol-gel procedure was used to form MgO nanoparticles which were used to adsorb Reactive Red 21 [52], with a maxium adsorption loading of 385 mg/g at a pH range of 5–9, and 20 min of contact time. Dye-bearing MgO nanoparticles was regenerated at 500° C during two hours and reused with a reasonable efficiency (pink colour appeared in the solution after the sixth cycle, increasing in colour within the seventh cycle). These MgO nanoparticles presented a 98% dye removal from a real textile wastewater (formed as in [50]).

CuFe-LDH/g-C_3N_4 (CFL/CN) nanocomposites were prepared and investigate to remove Alizarin Red S, and the results were compared with the derived from the use of CFL/CN nanoadsorbent [53]. Sono-CFL/CN nanoadsorbent was more effective (near 96%) on the removal of the dye in comparison to hydro-CFL/CN nanomaterial (53%). Maximum dye uptake was in the 65-75 mg/g range, which was dependent on the technology used to remove the dye. Sono-CFL/CN lost its initial adsorption capacity under continuous use (Table 2).

 doi:10.20944/preprints202405.1122.v1

Table 2. Percentage of reusability of SONO-CFL/CN nanomaterial.

Cycle	Adsorption	Sono-sorption
1st	78.4	96.2
2nd	60.4	87.6
3rd	59.9	76.5
4th	57.4	74.7

1. Experimental conditions: 0.02 g adsorbent/50 mL solution. Time: 30 min. Temperature: 25º C. Initial dye concentration: 20 mg/L. pH: 2.0±0-5. From [53].

A nanostructured composite based on superparamagnetic iron oxide nanoparticles (SPIONs), coated with hydroxyapatite (HAp), was show to be a good adsorbent against the presence of Congo Red in aqueous solutions [54]. Amongst the various formulations, the composite containing 35 wt.% of SPION was selected to adsorb the organic dye. Results concluded that the best efficiency on the removal of the dye were achieved when 0.10 g of SPION/HAp treated 50 mL of a solution containing 50 mg/L of the dye at pH 0 and a contact time of four hours. The maximum Congo Red adsorption uptake using the SPION/HAp adsorbent was determined to be 158.98 mg/g. The composite can be separated from the solution using magnets.

Ion gelation procedure was used to fabricate chitosan nanoparticles which were used on the removal on the removal of anionic dyes (Reactive Yellow 145, Reactive Blue 19, and Reactive Red 195) from solutions [55]. The utilization of polyaluminium chloride (PAC) (80 mg/L) and chitosan nanoparticles (150 mL/L) at pH= 6.6 produced the maximum (92%) color removal efficiency. Thus, with the use of chitosan nanoparticles, the amount of PAC needed to increase the color removal efficiency was reduced. Furthermore, the effect of chitosan nanoparticles on the adsorption of the dyes revealed that the Langmuir type II isotherm equation was followed, with a maximum adsorption capacity of 1100 mg/g.

This reference [56], investigated the production of amorphous biochar from breadfruit leaves, product which was utilized to remove Congo Red from solutions. The average size of the char was of 190 nm, however, after the adsorption of the dye the average size increased to 460 nm. The adsorption of Congo Red was studied under different dye concentrations (5-50 mg/L), reaction time (30 min-four hours), pH (6-9), and char dosages (0.5-2 g/100 mL). RSM-BBD design results showed maximum removal efficiency (99.96%) at pH 6.37, dye concentration of 45 mg/L, time 105 min, and biochar dosage of 1.92 g. Adsorption data fitted well to the Langmuir Type-II isotherm with maximum upload of almost 18 mg/g.

A nanobiosorbent was fabricated via microwave crosslinking of nanosilica gel with banana peels nanobiochar (BPNB) and chitosan hydrogel (Chit Hgel) to produce BPNB-NSiO$_2$-Chit Hgel nanobiosorbent (22.48–26.23 nm) [57]. The influence of nanobiosorbent dosage (1–50 mg), pH (2–12), reaction time (1–45 min), dye concentration (5–100 mg/L), temperature (15-60º C), and interfering salts on the adsorption of Congo Red was investigated. Maximum dye uptake were about 58 mg/g. Removal of the dye (92.8–95.0 %) from tap, sea, and wastewater can be reached.

Zinc ferrite ($ZnFe_2O_4$, BET surface area 85.88 m2/g) and copper ferrite ($CuFe_2O_4$, BET surface area 41.81 m2/g) nanoparticles were formed, and used as adsorbents, in the removal of Alizarin Yellow R, Thiazole Yellow G, Congo Red, and Methyl Orange from industrial wastewater [58]. The use of acidic pH values favoured the removal of the dyes, being the maximum monolayer adsorption capacities higher using zinc ferrite than copper ferrite (Table 3).

Table 3. Dyes uptake (mg/g) using zinc or copper ferrites in nanoparticulated form.

Nanoparticle	Alizarin Red S	Thiazol Yellog G	Congo Red	Methyl Orange
$ZnFe_2O_4$	54.6	37.0	29.8	26.8
$CuFe_2O_4$	46.4	30.1	21.9	20.8

From [58].

 doi:10.20944/preprints202405.1122.v1

In this work [59], multifunctional Fe_3O_4@N-C (nitrogen-doped carbon) nanocomposites with hollow porous core-shell structure were formed by different procedures. These included, i) hydrothermal method, ii) polymer coating, iii) thermal annealing process in nitrogen and iv) etching step in HCl medium. Fe_3O_4@N-C nanocomposites etched by HCl for different lengths of time, especially Fe_3O_4@N-C-3 (30 min of etching time) nanocomposites, also adsorbed Methyl Orange (98.7 % after 100 min).

Sodium alginate/gellan gum and polyethyleneimine were utilized to fabricate a material with 3D hierarchical porous architecture and used in the removal of Congo Red from waters [60]. The aerogel showed an adsorption uptake of 3 g/g, selectively separate Congo Red in the presence of other dyes from binary systems: Congo Red plus Amaranth (anionic dye), or Safranine T (cationic dye), or Methyl Orange (anionic dye) or Rhodamine B (cationic dye). From single dye solutions, the affinity of the aerogel from the dyes followed the order: Congo Red> Rhodamine B> Methyl Orange> Amaranth> Safranine T. After three cycles, the adsorption capacity decreased by 14.8%, maintaining an adsorption capacity of near 0.5 g/g (0.65 g/g in the first cyle).

Congo Red was removed, from solution, using green pea peels biochar (GPBC), and zinc oxide green pea peels biochar nanocomposite (ZnO/GPBC, particle size 14.58 nm) [61]. The experimental conditions used in the investigation were: dye concentration (50–250 mg/L), GPBC and ZnO/GPBC dosage (50-250 mg/100 mL), pH (2−12), temperature (20–60o C) and time (0–90 min). The results showed that ZnO/GPBC was more effective to remove the dye than GPPBC (98% versus 90%, respectively) under the optimized conditions. The monolayer adsorption capacities were 114.94 mg/g and 62.11 mg/g for ZnO/GPBC and GPBC, also respectively. In both cases, there was a decrease in the dye removal capacity with the number of cycles: ZnO/GPBC (98.4% in the first cycle against 88.8% in the fifth cycle), GPBC (90.4% first cycle versus 76.2% fifth cycle).

The removal of Congo Red, from mimic wastewater, was used to evaluate the properties of different composition ratios of CMC-nZVI (nano zero-valent iron coated with carboxymethyl cellulose) [62]. At an initial dye concentration of 500 mg/L, the increase of CMC contents favoured the decolorization process. The removal efficiency were of near 100%, at the CMC:Fe^{2+} ratio of 0.004 within 10 seconds after the addition of CMC-nZVI to the dye solution, whereas the optimal decolorization rate (90%, with an uptake capacity of near 8 g/g) was observed when the iron concentration was of 1 g/L. The above results were attributable to the break of the chromophore groups (-N[dbnd]N-), responsibles of the color of the dye, to N–H bonds.

F-Ln (Ln= Ce, Pr and Nd) nanosheets, provided of surface acetates groups, were prepared through a hydrothermal synthetic methodology at room temperature and pressure, and used in the adsorption of Congo Red and Coomassie Brilliant Blue G-250 anionic dyes [63]. The maximum Langmuir adsorption capacities for the respective two dyes were 4334 mg/g and 2827 mg/g. Both dyes, loaded onto the adsorbent *via* its exchange with the surface acetates groups of the F–Ce nanosheets. Furthermore, these nanosheets presented a salt-tolerance in saturated NaCl medium or elevated concentrations of Na_2SO_4, K_2CO_3 and $NaNO_3$ in the solutions.

2.2. Photo)-Catalytic Degradation of Anionic Dyes Using Nanomaterials

By means of *Moringa stenopetala* seed extract, copper oxide nanoparticles (average particle size 6.6 nm) were formed and used to degrade Congo Red and Alizarin Red S [64]. After two hours of exposure to irradiation and varying experimental conditions, Congo Red degraded near 98%, whereas the degradation of Alizarin Red S reached 95%. The continuous use of the catalyst for five cycles also was investigated, and in both cases, the adsorbent lost its effectiveness after each cycle.

Under a chemical precipitation procedure, zinc oxide (ZnO), copper ferrite ($CuFe_2O_4$) and the zinc oxide-copper ferrite binary composite were prepared, following by the formation of a ternary composite (ZnO-$CuFe_2O_4$-CNTs) [65]. These compounds were used to search the photocatalytic degradation of Congo Red under sunlight exposure, reaching 82% dye degradation in two hours. ZnO-$CuFe_2O_4$-CNT nanocomposite had better degradation efficiency than the pure oxides and their binary composite.

 doi:10.20944/preprints202405.1122.v1

Bi_2O_3-NiO heterojunction was formed from the respective Ni(II) and Bi(III) nitrates and used to degrade Methyl Orange under visible-light exposure [66]. The photocatalytic degradation of the dye reached rates of 46% (nickel oxide), 67% (bismuth oxide) and 100% (mixed nickel-bismuth oxide). Transfer of positive holes and electrons and the separation being the responsible for the better activity of the mixed oxides heterojunction, which *apparently* can be recycled several times, as written in the published Abstract, however these data did not appear in the publication.

Bi_2WO_6 nanomaterials, containing a chelating agent (EDTA), were used to degrade Methyl Orange and Congo Red in the presence of $NaBH_4$, being the catalytic efficiency of Bi_2WO_6 surpassed by that of the EDTA-Bi_2WO_6. This catalyst could be recycled up to five times without undergoing a significant loss in activity [67].

Carbohydrate conjugated Ag, Au and Ag-Au alloy biocompatible nanoparticles (14.5, 11.7 and 16.3 nm respective average particle size) had been fabricated through bio-reduction of the metal salts in the presence of *Lobaria retigera* (high altitude lichen) [68]. These nanoparticles acted as catalysts for the degradation of Methyl Orange.

In order to control its characteristics, β-cyclodextrin and honey were used, as surfactants, during the synthesis of ZnO nanoparticles, which were coupled with silver to form ZnO-xAg, ZnO-C-xAg and ZnO-H-xAg binary structures with typical crystalline sizes of 9.38 nm [69]. The photodegradation of Bromophenol Blue showed increased photoactivity upon modification with cyclodextrin, honey, and silver nanoparticles. Dye photodegradation was near 100% by the use of ZnO-H-3Ag (3 wt% silver).

Ti_3C_2 MXene and its nitrogen-doped derivative (N-Ti_3C_2 MXene) were used in the removal of Methyl Orange from waters [70]. The results indicated that the catalytic efficiency of N-Ti_3C_2 MXene increased near ten times in comparison with the corresponding of the Ti_3C_2 MXene nanomaterial. N-Ti_3C_2 1:8 MXene composition performed best, since the degradation of a 20 mg/L dye solution reached more than 98% after twenty minutes of UV lamp irradiation. The effectiveness of this material was attributable to the presence of more abundant surface functional groups, improving the charge transfer efficiency and enhance the electrical conductivity of the catalyst.

Ag/Mn–ZnO nanomaterial (4-5 nm) was used to remove Methyl Orange and Alizarin Red S from solutions, both dyes degraded near 70% after 100 min of reaction time [71]. However, and in the case of Alizarin Red S, the nanomaterial did not maintain intact its degradation efficiency until continuous use (five cycles).

2D borate anions $B_4O_5(OH)_4^{2-}$ intercalated layered double hydroxide (ZnGa-BLDH) nanosheets (5–6 nm) were investigated in the photodegradation removal of Congo Red from aqueous environment [72].

The aqueous extract of *Ulva lactuca* and ZnO nanopowders were used to fabricate ZnO@C nanocomposites, material which was investigated to degrade Congo Red under UV and visible light exposure [73]. This nanocomposite degraded better the dye than the pristine zinc oxide nanopowder.

Undoped TiO_2 and Fe-doped TiO_2 materials, prepared *via* sol-gel and precipitation procedure, were used as photocatalysts to remove Methyl Orange under UV-A and visible-light irradiations [74]. The photocatalytic experiments revealed an increase of the photocatalytic activity of 0.5%wt Fe-doped TiO_2 composition, and only under UV-A light, compared to the rest of the prepared nanomaterials. This increase was due to the efficient charge separation of electrons and holes.

Iron oxide nanoparticles (IONPs, composed of amorphous FeOOH and FeII/III-polyphenol complexes)) with extracts of the plant *Camellia sinensis*, were used to remove Methyl Orange from solutions [75]. The nanoparticles were used as heterogeneous-Fenton catalysts for the removal of the dye. Best results were obtained at pH values around 3.

Graphene oxide nanosheets-yttrium oxide (Y_2O_3)–silicon oxide (SiO_2) ternary nanostructures were fabricated to investigate its photo-degradation activity against the presence (20 ppm) of Methyl Orange in aqueous solutions [76]. The photo-degradation of the dye improved from 1.17% for Y_2O_3/SiO_2 nanostructures to 52% when the concentration of the graphene oxide nanosheets reached 15 wt% and 45 min of reaction time.

 doi:10.20944/preprints202405.1122.v1

Pristine Fe_2O_3, 1 wt% metal (Ag, Co, and Cu) doped Fe_2O_3 nanoparticles (NPs) were fabricated using a hydrothermal and wet impregnation method [77]. The nanoparticles were employed as photosensitizers for the degradation of Reactive Red and Orange II dyes under sunlight irradiation. The synthesized 1 wt% Ag–Fe_2O_3 (AgF) NPs had the best catalytic properties, compared with pristine Fe_2O_3 and CoF and CuF, to degrade (98.32%) both dyes within 120 min of reaction time.

The photocatalytic properties of polymeric g-C_3N_4 layers coated with various dosages of erbium oxide nanoparticles were investigated on the oxidation of Orange G under visible-light exposure. The nanoparticles maintained its activity above 95% up to three cycles of reusability [78].

ZnO-ZnS-CdO-CdS quaternary core-shell nanocomposites (NCs) were fabricated using *Ricinus communis* as stabilizing agent and hydrazine hydrate as reducing agent [79]. The nanocatalysts were used in the degradation of Congo Red and Methyl Red dyes, being active both in the degradation of single or a mixture of the dyes.

The removal of Congo Red, under UV light in the presence of H_2O_2, and the photocatalytic activity of copper oxide nanoparticles (CuONPs, 25-90 nm size) were investigated [80]. The UV light decomposed H_2O_2 with formation of ·OH radicals, which improved the degradation of the dye. This degradation occurred by reaction of the dye with the radicals, though other reactions of the dye with i.e. a positive hole (h^+_{vb}), contribute to the elimination of this harmful compound.

A one-step laser technology was used to fabricate boron, doped and boron and nitrogen co-doped highly reduced graphene oxide and multiwall carbon nanotubes/Ni oxide and Ni hydroxide nanohybrid layers [81]. These materials were employed to investigate its properties on the photocatalytic removal of Methyl Orange. The best photocatalytic activities resulted for boron and nitrogen co-doped materials formed by the use of H_3BO_3 and urea as boron and nitrogen precursors, respectively; however, the degradation efficiency failed after continuous use: 80% in the 1st cycle and 3% in the third cycle.

Direct thermal polymerization procedure was utilized in the fabrication of 1D/2D g-C_3N_5/g-C_3N_4 heterojunction (1D/2D-N_5/N_4) used in the removal of Methyl Orange from wastewater [82]. 1D/2D-N_5/N_4 had one-dimensional g-C_3N_5 nanorods and two-dimensional g-C_3N_4 nanosheets. The photocatalytic degradation of the dye reached a rate of 99.6 %, maintaining a 92.20 % after five cycles.

Attapulgite (ATP) mineral nanomaterials grafted with magnetic Fe_3O_4 nanoparticles, with a further modification with polyethyleneimine (PEI), served to the fabrication of functionalized magnetic attapulgite composites (ATP-Fe_3O_4-PEI), which was utilized for the removal of Congo Red from wastewater [83]. The removal of the dye by means of the nanocomposite was attributed to a catalytic degradation process. However, without photoirradiation and the presence of oxidants in the solution, the system formed H_2O_2 and hydroxyl radicals (·OH) to catalytically degraded dye molecules. Moreover, the removal of the dye was further increased by adsorption on the composite material through electrostatic attraction, hydrogen bonds, and π-π interaction. Under two removal tests, the removal rate of the dye exceeded 95%, corresponding to a removal capacity of 943.77 mg/g, at pH 3 and 25° C. This composite presented removal effectiveness and uptake capacity exceeding 82% and 799 mg/g, respectively, after four cycles.

The efficiency of Mn-20wt%Ni and Mn-30wt%Ni particle powders in relation to the degradation of Reactive Black 5 as function of different experimental variables was investigated [84]. Mn-20wt%Ni particles presented better degradation efficiency and faster rate of reaction than Mn-30wt%Ni material.

The metal assisted chemical etching (MACE) technique was used to produce SiNWs-NiNPs/NiONPs [85], these nanoparticles were used to the photocatalystic assisted degradation of Methyl Orange from an aqueous solution. The degradation of 20 ppm of the dye had an efficiency of 66.5% after three hours and under UV exposure.

Manganese oxide (MnO_2)/silicon carbide (SiC) nanostructures doped polystyrene (PS)–polycarbonate (PC) blend was used to investigate its properties to degrade Methyl Orange [86]. Results indicated that the use of PS–PC/MnO_2–SiC nanocomposites, under UV-exposure, removed the dye colour with an efficiency of near 54% within 90 min, and using the 5.2 wt% MnO_2/SiC NPs formulation.

 doi:10.20944/preprints202405.1122.v1

Carbon dots with diameters of 4.9±1.5 nm and 4.1±1.2nm were fabricated from nitric and sulphuric acids, respectively, and *Ilex paraguariensis* as raw material [87]. These dots were used to fabricate magnetite-containing nanocomposites, being these nanocomposites utilized to investigate the photocatalytic degradation of Methyl Orange. At pH 6.2, 8.5 ppm dye concentration and 100 ppm nanomaterials doses, all the above nanocompounds presented catalytic activity allowing the removal of up to 98% dye under visible irradiation (400 nm) and seven hours of reaction.

Cetyltrimethylammonium bromide surfactant assisted hierarchical TiO_2 heterojunction was doped with europium to form a nanostructure with crystallyte sizes in the 4-10 nm range [88]. Further, Congo Red dye was photocatalytic degraded within the above materials in the presence of UV ligh, increasing the degradation rate with the reaction time. After 75 min, the efficiency in the dye degradation reached 97%; it was also concluded that the degradation is dependant on the dispersion of the nanomaterials.

Multifunctional surface-modified CuO nanomaterials were used for the degradation of AR88 dye. At pH 11, the nanomaterial degraded near 95% of the dye under UV exposure, and utilizing 1 g/L nanomaterial dose [89].

Zinc oxide/copper oxide nanocomposites (ZnO/CuO NCs) presenting various proportions of binary oxides were investigated for the degradation of Congo Red [90]. Experiments carried out on dye-bearing water and real textile wastewater, under visible light irradiation by 0.5 M ZnO:0.5 M CuO nanocomposite, showed both acting as catalysts by tuning doping concentration of copper oxide in ZnO.

Polymethyl methacrylate (PMMA)-polycarbonate (PC)/antimony oxide (Sb_2O_3)-graphene oxide (GO) nanocomposites films were fabricated [91]. These nanomaterials were used in the photodegradation of a 20 ppm Methyl Orange solution. This degradation was due to a rise in electron–hole pairs and a reduction in fix replication.

This reference investigated a ceramic-based nanomaterial catalyst (a reduced graphene oxide-ZnS, rGO-ZnS) for the oxidative photocatalytic degradation of Naphtol Blue Black dye solution under exposure to sunlight [92]. The dye was degraded (93.7%) under exposure to direct solar light.

SiO_2/g-C_3N_4 photocatalyst was fabricated, fixing the amount of SiO_2, and varying the concentration of graphitic carbon nitride in the ratio (1:x, where x= 1, 2, 3); these nanocomposites were used to investigate their photocatalytic properties to degrade Auramine O and Xylenol Orange dyes [93]. The results showed that SCN_2 (x= 2) nanocomposite improved the photocatalytic activity, under visible light exposure, with degradation efficiencies of 70% and 84.6% for the respective above dyes, being these results attributable to the large surface area and the electron–hole separation rate that the nanocomposites presented.

Bismuth oxychloride (BiOCl) nanoplatelets and lignin-based biochar were used as precursors to fabricate composites formed by bismuth oxyhalide nanoparticles, being investigated the simultaneous photocatalytic and adsorptive efficiency of the Biochar–BiOCl (%BC-BiOCl) composites on the removal of Methyl Orange [94]. The maximum dye removal and degradation (100%) was reached under the next experimental conditions: composite dose of 1.39 g/L, initial dye concentration of 41.8 mg/L, pH of 3.15, and one hour of reaction under light exposure. Similarly to other nanomaterials, there was an efficiency lost after various cycles; in this case the efficiency dropped from 99% in the 1st cycle to 63% in the fifth cycle (1 g/L of 15BCPC dosage, 30 mg/L initial dye concentration at pH 5).

1-hexyl-3-methyl-2-(2-oxo-ethyl)-3H-imidazol-1-ium bromide (HMIB) ionic liquid embedded on CdO-TiO_2 (HMIB-CT) hybrid nanomaterial was used in the removal of Tripan Blue dye from solutions [95]. Complete dye removal under natural sun beam irradiation, required for the photocatalytic activity, was accomplished at pH 7 and one hour of reaction time.

After the formation of the magnetic photocatalyst *Scendesmus sp.*/Fe_3O_4/TiO_2, its sonophotocatalytic properties with respect to the degradation of the Red195 dye were investigated [96]. At pH of 5, photocatalyst dosage of 100 mg, initial dye concentration of 100 mg/L, ultrasound power of 38W, and an exposure time of 20 min, the maximum Red195 removal efficiency (100%) resulted. After five cycles of recycling, the degradation efficiency remained above 95%. Experiments

 doi:10.20944/preprints202405.1122.v1

on scavenging indicated that electrons (h+) and OH^- groups were necessary to act as decomposition reagents.

2.3. Remarks to the Use of Nanomaterials in the Removal of Anionic Dyes from Solutions

Whereas subsections 2.1. and 2.2. show that two approaches are using by scientists to remove anionic dyes from solutions: adsorption or (photo)-catalysis, Table 4 summarized the various anionic dyes object of these investigations. For the number of references, it is clear that (photo)-catalytic degradation of organic dyes is the methodology of preference against the use of adsorption-elution to fit this environmental task. In any case, it is difficult to compare results due to the various experimental conditions used in each reference. Using (photo)-catalysis, the degradation of the dye occurs at the few minutes or hours (see Table 5), whereas in the case of adsorption procedures, dye uptakes vary from a few mg/g to the g/g order (see text and also Table 10).

Table 4. Summary of the use of nanomaterials in the removal of anionic dyes.

Methodology	Anionic dye	Reference
Adsorption	Acid Yellow 36, Acid Orange 6	[49]
	Reactive Red 21, Reactive Blue 19	[50,52,55]
	Congo Red	[51,54,56,57,60–63]
	Alizarin Red S	[53]
	Reactive Yellow 145, Reactive Red 195	[55]
	[a]Various (industrial wastewater)	[58]
	Methyl Orange	[59]
	Congo Red, Brilliant Blue G-250	[63]
-	Congo Red, Alizarin Red S	[64,65,67,71–73,79,80,83,88,90]
	Methyl Orange	[66–68,70,71,74–76,81,82,85–87,91], [94]
	Brilliant Blue	[69]
	Reactive Red, Orange II	[77]
	Orange G	[78]
	Congo Red,Methyl Red	[79]
	Reactive Black 5	[84]
	AR88	[89]
	Napthol Blue Black	[92]
	Auramine O, Xylenol Orange	[93]
	Tripan Blue	[95]
	Red 195	[96]

[a] Alizarin Yellow R, Thiazole Yellow G, Congo Red, and Methyl Orange.

From the above, just one reference, [58], utilized a real industrial wastewater in the investigation, also, his Table shows that Congo Red and Methyl Orange are the most investigated anionic dyes, .

 doi:10.20944/preprints202405.1122.v1

Table 5. Some efficiencies in the removal of anionic dyes using (photo)-catalysis.

Dye	Nanomaterial	Efficiency-time	Reference
Congo Red	Cu oxide nanoparticles	93%-2 hours	[64]
	ZnO-$CuFe_2O_4$-CNTs	82%-2 hours	[65]
	Eu-TiO_2	97%-75 min	[88]
Methyl Orange	N-Ti_3C_2MXene	98%-20 min	[70]
	Y_2O_3-SiO_2	52%-45 min	[76]
	Various nanomaterials	67%-3 hours	[84]
	Carbon dots	98%-7 hours	[87]
	Biochar-BiOCl	100%-1 hour	[94]
Reactive Red	Ag-Fe_2O_3	98%-2 hours	[77]
Orange II	Ag-Fe_2O_3	98%-2 hours	[77]
Tripan Blue	Cd,Ti oxides-Ionic liquid	100%-1 hour	[95]

3. Nanomaterials and Cationic Dyes

3.1. Adsorption of Cationic Dyes on Nanomaterials

Two different processes (Calix-MNPs and Calix-Si-MNPs) were used to modify magnetite nanoparticles with p-sulfonatocalix[6]arene and were used for the removal of Crystal Violet from aqueous solution [97]. Calix-Si-MNPs showed a better adsorption capacity than Calix-MNPs, attributable to the modification on the surface of magnetite nanoparticles through a spacer. The nanoadsorbent can be recovered using a magnet, however, there was a considerable lost of capacity up to four cycles of adsorption (pH 7)-desorption (water plus acetone).

In this work [98], amorphous and crystalline products based on Zr, Mg, and Mn were fabricated through the Pechini sol–gel procedure and used to remove Basic Fuchsin dye from solutions. Samples fabricated before calcination was amorphous, whereas the samples calcined at 500° C or 700° C presented mean diameters of 45.16 nm and 76.28 nm, respectively. Figure 1 showed that increasing the temperature of calcination the dye uptake onto the nanomaterials decreased. Maximum dye uptake varies in the 93-240 mg/g concentrations range.

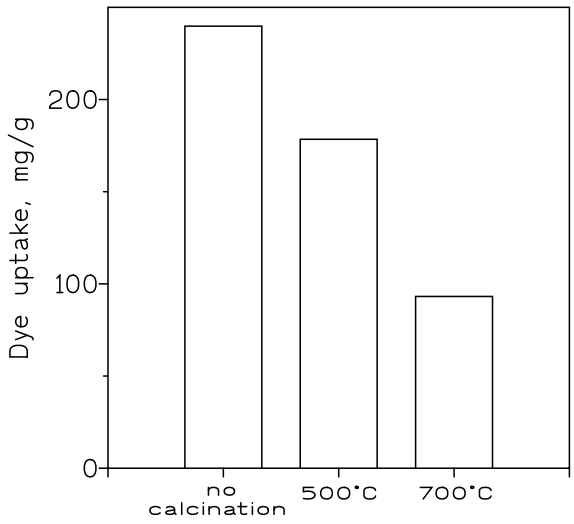

Figure 1. Influence of the calcination temperature on Basic Fuchsin uptake. From [98].

Succinic anhydride modifying the surface of native cellulose nanocrystals was used to adsorb Golden Yellow and Methylene Blue. No data about the desorption step were given in the work [99].

 doi:10.20944/preprints202405.1122.v1

Bionanocomposites formed of chitosan grafted by various monomers, such as acrylamide, acrylic acid, 4-styrene sulfonic acid, and hybrid nanoparticles of graphene oxide/titanium dioxide nanoparticles (GO@TiO_2-NPs) were fabricated and used in the adsorption of Basic-Red 46 [100]. The removal of the dye from the aqueous solution followed the pseudo second-order kinetics and Langmuir isotherm models, with maximum upload in the 43-79 mg/g range..

Food industry waste hazelnut shells were used as precursors to prepare, via impregnation with $ZnCl_2$ followed by chemical activation with KOH, porous carbon materials to be used as adsorbents of a Methylene Blue-wastewater [101]. The Fusso effect, which can reduce the size of the dye molecules, increased the adsorption properties of the carbon. The material showed a dye uptake of 694.03 mg/g, which can be increased to 882.46 mg/g in 0.1 M NaCl medium.

Calcium silicate nanopowders were fabricated from marble sawing dust and silica fume using microwave irradiation-assisted route. These nanomaterials were investigated in the removal of Malachite Green from solutions in the pH 2-12 range, with best results yielded (near 100% removal) at the pH of 12. Adsorption data fitted well with the linear form of the Freundlich isotherm. Dye-desorption was investigated by the use of acetone; after continuous adsorption-desorption cycles, it was shown that after six cycles the adsorption efficiency decreased from 100% (first cycle) to 78% (sixth cycle). This decrease attributable to the decrease in the number of the surface-active sites after continuous use [102].

Under the polyol process, FePt nanoparticles with a size less than 2 nm, were uniformly distributed over the surface of hexagonal boron nitride nanosheets. These materials were used in the adsorption of Methylene Blue, Methylene Violet and Brilliant Green [103]. The removal of the dyes from the solution depended on the composition of the nanomaterial used in the experimentation and the annealing temperature (Figure 2). However, no data about the desorption step were provided in the published manuscript.

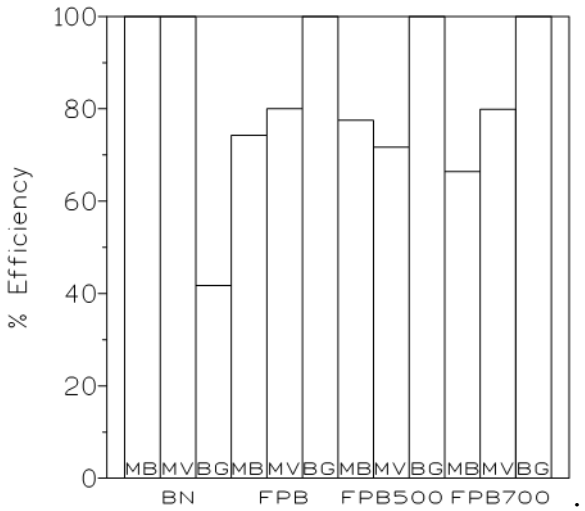

Figure 2. Efficiency in the removal of Methylene Blue (MB), Methylene Violet (MV) and Brilliant Green (BG), after 24 hours, with different FePt/h-BN heteromaterials. BN: boron nitride. FPB: as-synthesized. FPB500: annealed at 500º C. FPB700: annealed at 700º C. From [103].

A nanomanufacturing process which included the treatment of α-chitin nanocrystals (ChNCs) by electron-beam irradiation, EBI-induced ChNCs, with nano-sized and rod-like morphology with tunable lengths averaging 259-608 nm and uniform widths of 12-16 nm, were formed [104]. The anionic groups presented in the nanomaterials reacted with Toluidine Blue O dye via electrostatic attraction, forming hydrogels, which were self-supporting after centrifugation. No desorption data were included in the manuscript.

Nano-sized polylactic acid was decorated on the surface of graphene oxide to investigate it performance on the removal of Methylene Blue from an aqueous solution [105]. Optimum adsorption parameters were: adsorbent dosage of 0.5 g/L, pH 4, reaction time of two hours, and 45º C. Data fitted

 doi:10.20944/preprints202405.1122.v1

with the Langmuir isotherm with maximum uptakes in the 104-224 mg/g range. Experimental results showed that the loading capacity of the polylactic acid-graphene oxide nanoadsorbent increased near 70% in comparison with that of sulphur oxide. The nanoadsorbent presented a loss of near 27% adsorption efficiency after five cycles.

Using the co-precipitation method, superparamagnetic iron oxide nanoparticles (SPIONs) with size of 13.6±1.9 nm were synthesized [106]. Further, the surface of SPIONs was modified by polyvinyl alcohol, chitosan, and graphene oxide, and the modified nanomaterials were used to adsorb Methylene Blue. Removal efficiency at pH 7 reached near 87% after 13 days, and the highest dye loading capacity was 3.6 mg/g, while the highest loading amount achieved was 36.4 mg/g. The cumulative desorption capacity of the adsorbent at pH 3.8 was at its maximum at almost 9.0% after 30 days.

Tin oxide nanorods and SnO_2/MoO_3 nanocomposite were fabricated, via the use of the leaf extract of *Magnifera indica*, the presence of polyphenols in the extract facilitated the reduction of the precursor metal salt to the corresponding oxide [107]. The catalytic properties of the above materials were investigated on the degradation of Methylene blue. The photocatalytic efficiency of the mixture of oxides improved to 73% as compared to that of SnO_2 (69.0%).

In this reference [108], Zn-modified biochar obtained from zinc carbonate and Jerusalem artichokes straw was used to explore its effect on the adsorption of Methylene Blue. Compared with the original biochar, the specific surface area (1037.17 m^2/g) of the Zn-modified biochar by pyrolysis at 800° C (Zn-BC 800) increased approximately 22 times. The adsorption of Methylene Blue with Zn-BC 800 followed the pseudo-second-order kinetic model. At 45° C, Zn-BC 800 had a maximum adsorption loading of 477.13 mg/g. Hydrogen bond and π-π interaction were the main responsible for the dye adsorption onto Zn-BC 800. The adsorbent lost its initial dye uptake of near 420 mg/g until 350 mg/g in the fifth cycle, in these series of experiments, anhydrous ethanol and distilled water were used as eluent.

Yellow phosphorus slag was used to develop a SiO_2 matrix material, which was loaded with MgO, and then the formed composite was investigated as adsorbent of Malachite Green dye [109]. These investigations demonstrated that when using this composite, a maximum dye adsorption rate of 97.72 % was reached, with a dye uptake of 115.64 mg/g, experimental data responded well to the Freundlich isotherm. In this case, 0.1 M sodium chloride medium was utilized to desorb the loaded dye, after four cycles of continuous use there was a slight decrease in the adsorption efficiency.

3.2. Nanomaterials–Forming Membranes for the Removal of Cationic Dyes

A ZIF-67/SA@PVDF (ZSA3@PVDF) mixed matrix membrane had been produced by incorporating silicon aerogel (SA) and zeolitic imidazolate framework material 67 (ZIF-67) nanoparticles in a polyvinylidene fluoride (PVDF) membrane [110]. By the use of this membrane, Methylene Blue removal rate exceeded 99% when filtrating 100 mL of a 5 mg/L dye solution. The continuous use of the membrane showed that its removal efficiency was maintained above 98% after three cycles of the dynamic adsorption process.

3.3.(. Photo)-Catalytic Degradation of Cationic Dyes Using Nanomaterials

Pure Fe_2O_3 (FO with 46 nm particle size) and a series of 5%, 10% and 15% Ni doped Fe_2O_3 (5-NFO, 10-NFO and 15-NFO) nanoparticles (19 nm particle size) were synthesized to investigate the effect of nickel concentration on the photocatalytic activity on Methylene Blue degradation [111]. The highest dye degradation was yielded using 10-NFO nanoparticles and 100 min of reaction time. The optimal concentration of 10-NFO accelerated the photoreduction of the dye due to the photocatalyst characteristics to trap electrons.

Pristine Fe_2O_3 hematite and Nb-doped Fe_2O_3 nanostructures with different doping concentrations of 5%, 10%, and 15% of niobium, were used to investigate the degradation of Methylene Blue [112]. After 100 min of exposure to visible light, the highest level of dye degradation was attained by 10%-NFO composition. The photocatalytic properties of doped Fe_2O_3 was attributed to a decrease in band gap energy.

 doi:10.20944/preprints202405.1122.v1

$Mn_4(P_2O_7)_3$ nanoflakes were synthesized and used to remove Methylene Blue from water [113]. The electrostatic interaction between the negatively charged group of the nanoflakes and dye cationic molecules ruled the adsorption process; further, the dye was degraded *via* a heterogeneous catalytic process performed at basic pH in the presence of H_2O_2 and reactive oxygen species production. After 30 min and using an initial dye concentration of 40 mg/L, the degradation rate reached 99.2%.

Rhodamine B was degraded by a photocatalytic process, under direct sunlight, by the use of sol-immobilization synthesized monometallic (Pd and Au) and bimetallic (Pd-Au) hybrid nanomaterials supported on reduced graphene oxide (rGO) [114]. Bimetallic Au-Pd-rGO composites had better catalytic efficiencies than mono-metals-rGO nanomaterials. Under the best formulation (Au0.75-Pd0.25/rGO), the degradation efficiency reached 98%, whereas the nanocomposite can be used for five cycles maintaining 89% of its activity.

The degradation of Methylene blue and Rhodamine B had been investigated using cadmium sulfide nanoparticles (CdSNPs, average size less than 20 nm) encapsulated by natural extract [115]. These nanoparticles were synthesized *via* green chemical reduction route that uses natural stabilizers such as rice water, papaya fruit extracts and precursors such as cadmium chloride, cadmium nitrate, and cadmium sulphur.

Cerium doped cobalt-magnesium ferrites $Co_{0.7}Mg_{0.3}Ce_xFe_{2x}O_4$ were prepared and used to investigate its potential as degrading agent against Methylene Blue [116]. The nanocomposite with x= 0.1 presented a degradation efficiency of near 95.5% in one hour, with free radicals $O_2^{\cdot-}$and $OH^{\cdot}$ acting as the active species to promote dye degradation, which produced CO_2 and water as final products. This material presented a near constant recyclability efficiency after five cycles (95.5%-94.8%).

The next investigation used ZnO–NPs from milky sap of *Calotropis procera* parts to degrade Malachite Green and Methylene Blue under UV-light exposure [117]. The degradation efficiency reached 85.3% (Malachite Green) and 86.3% (Methylene Blue), being, in both cases, increased the efficiency from pH 4 to pH 10.

A soft nanocomposite hydrogel, comprising a pyrene-based chiral amphipath having an amino acid (l-phenylalanine) core with pendant oligo-oxyethylene hydrophilic chains and sulphur oxide, was used in the degradation of Methylene Blue and Rhodamine B [118]. Experimental results indicated that the removal efficiency was better in the case of Methylene Blue than Rhodamine B.

Montmorillonite K30 nanosheets were decorated with *Carrisa edulis* fruit extract capped spherical shape Co_3O_4 nanoparticles (size of 11.25 nm) to degrade methylthioninium chloride (Methylene Blue) [119]. Attributable to the generation of OH and O_2 radicals, the 20% loaded Co_3O_4 on MK30 nanocomposites had the best photocatalytic performance (near 98%) on exposing to visible light.

$0.2CoFe_2O_4/0.8TiO_2$-5%La nanocomposite was prepared, by a co-precipitation and hydrothermal process, to be used as a high activity photocatalyst for degradation of Methylene Blue under visible light irradiation [120]. This dye was degraded by 99% after 50 min of exposure time to the light.

Pure phased rare earth doped ZnO nanoparticles were fabricated for the degradation of Malachite Green and Crystal Violet [121]. For these dyes, the maximum degradation efficiency was near 98% when dysprosium doped ZnO nanoparticles were used to degrade the dyes. A tailored band gap and the presence of defects, which helped in the creation of a reactive species were the main responsible for dyes degradation.

Ionic mesoporous organosilica (IMOS) forming a polyethylene glycol (PEG)-linked bis-imidazolium chloride framework was prepared for the selective recovery of tungstate ions from wastewater and its further use as a photocatalyst against the presence of Rhodamine B in waters [122]. Under column experiments, a maximum recovery of tungstate ions (123 mg/g) was reached using a bed height of 3 cm and a flow rate of 3 mL/min. The use of this W(VI)-immobilized IMOS (W-IMOS), oxidized Rhodamine B through successive adsorption (30%) in the dark and photocatalytic degradation (66%) under UV-vis light irradiation.

Nanomaterials containing the $SrMoO_4/g\text{-}C_3N_4$ heterostructure were synthesized in a single step by the sonochemical method at controlled temperatures, further, these nanomaterials were used to

 doi:10.20944/preprints202405.1122.v1

degrade some cationic dyes [123]. The results of the photocatalytic investigations showed that the insertion of CN promoted photocatalytic degradation of Methylene Blue (99.58%), Rhodamine B (100%) and Crystal Violet (98.65%).

Two nanocomposites were prepared with varying compositions of ZnO and acid-activated kaolinite for use as photocatalysts to degrade Methylene Blue [124]. The ZK-30 nanocomposite (30 wt% ZnO) removed 98% of the dye from an aqueous solution of pH 10. The recyclability experiments about the continuous use of the nanocomposites showed 80–99 % dye removal for up to three consecutive photocatalytic cycles.

N/p-type nanomaterials loaded on the surface of cellulose nanoparticles had been used to fabricate hybrid nanomaterials to be used in the photocatalytic degradation of Methylene Blue and Rhodamine B dyes [125]. In single dye solutions, the degradation efficiency reached 95% for Methylene Blue and 47.4% in the case of Rhodamine B dye, whereas in a mixed dye solution the degradation reached 53% and 89.8% for Rhodamine B and Methylene Blue, respectively.

Titanium dioxide nanoparticles were prepared by a sol-gel process and calcined for 2 h at temperatures in the 300° C- 600° C range [126]. The increase of the calcination temperature produced an increase in the size of the nanoparticles. The photodegradation performance of these nanoparticles was investigated in the removal of 10 ppm Methylene Blue from water, showing the nanomaterial calcined at 400° C the best efficiency (near 95%) over the other nanoparticles examined in this work.

The tannic acid coating method was utilized to synthesize Ag nanoparticles-loaded ultralong hydroxyapatite (HAP). The nanowires were employed as building blocks together with chitosan (CS) to fabricate highly porous flow-through reactors (Ag@HAP/CS) for continuous catalytic reduction of Methylene Blue [127]. These nanomaterials presented efficiencies of near 99% at high fluxes, i.e. 2000 $L/m^2 \cdot h$, and using a very low concentration of $NaBH_4$ i.e. dye:$NaBH_4$ of 1.

Pseudobrookite (Fe_2TiO_5) was fabricated and used in the photocatalytic degradation of Rhodamine B [128]. The degradation process was associated with the adsorption of protons and the formation of an electron-hole pair. The nanomaterial thermally treated under nitrogen atmosphere presented better catalytic activity than those fabricated in air.

This reference [129], described the use of natural cotton substrates and the in situ mineralization of β-FeOOH nanorods as precursors in the synthesis of an inorganic–organic compound semiconductor nanomaterials (Cot-FeOOH). These materials had photocatalytic activity (98%) for Rhodamine B dye under visible light irradiation and in the presence of hydrogen peroxide.

Fe_3O_4 nanoparticles with a size of (350±50 nm) were synthesized by solvothermal method. Then, the nanoparticles were coated with a shell made of 3-aminophenol-formaldehyde (APF) resin to prevent agglomeration, and further, core–shell Fe_3O_4@APF nanospheres were produced by polycondensation within 10 min [130]. The magnetic Fe_3O_4@APF@Ag nanomaterials catalyzed the reduction, *via* the use of sodium borohydride, of Rhodamine B and Methylene Blue dyes, with conversion of these chemicals above 90% within 3 min of reaction time and a slight decrease in the reduction efficiency after seven cycles.

Ag_2O nanoparticles, with cubic structure and crystalline diameter of 18.5 nm, were prepared and used in the photocatalytic degradation of Rhodamine B [131]. The exposure of an aqueous solution containing the dye to UV-visible light during one hour produced a 76 % reduction of the compound. The main responsible in the degradation process were the reactions with super oxide radical ($O_2^{\bullet}$) and the hydroxyl radical ($^{\bullet}OH$).

Nanoparticles (average size of 1.87 nm) composed of Fe_3O_4/Mn_3O_4/CuO were used as nanocatalyst in the degradation of Methylene Blue under ultrasonic conditions [132]. The degradation of the dye was investigated under various experimental conditions, being the best of these conditions: temperature of 28° C, 0.03 g/L of initial dye concentration, 1.0 g/L of nanoparticles dosage, 5 mM of H_2O_2, and 60 kHz. A maximum of 95.04% dye degradation using these nanoparticles was reached after 150 min.

Using attapulgite (ATP) as carrier, Fe_3O_4 and g-C_3N_4 were grafted onto ATP, and the surface was then modified with polyethyleneimine (PEI) to produce photocatalyst ATP-Fe_3O_4-g-C_3N_4-PEI, which was used in the treatment of a Malachite Green-bearing wastewater [133]. Electron paramagnetic

 doi:10.20944/preprints202405.1122.v1

resonance analysis confirmed that the nanocomposite generated hydroxyl radicals (·OH) and superoxide radicals ($\cdot O_2^-$) which degraded the dye. Under the action of H^+, $\cdot O_2^-$, and ·OH, a removal rate of 98% was reached at pH 3. Recyclability experiments showed that there was a continuous degradation of the photocatalyst from the first (98% dye removal efficiency) to the fourth (65% dye removal efficiency) cycle.

The controlled synthesis of bismuth with various morphologies: nanoparticles (20-50 nm), nanorods (diameter of 20 nm and length 1 μm) nanocubes (150-200 nm) and micro-spheres (10 μm) has been investigated [134]. The degradation efficiency, after 90 minutes of exposure to visible-light irradiation, against the presence of Rhodamine B in solutions were 99.9%, 98.9%, 97% and 68.3% for the above morphologies, respectively. The catalytic activity of the same morphologies increased with the decrease of pH value, maintaining a removal rate of 73.5% after forty cycles. Remarkably, this is a work which investigates the reusability of these adsorbents for a number of cycles as high as 40, when the ordinary number rarely exceeded five cycles.

Superparamagnetic Fe_3O_4 nanoparticles synthesized via an electrochemical procedure were used as a catalyst for the oxidation of Rhodamine B in a photo-Fenton-like process [135]. The rate of color removal was 85% after 12 minutes at dye concentration of 2 mg/L, H_2O_2 concentration of 0.18 mM, and Fe_3O_4 concentration of 0.2 g/L. In addition, electrochemically synthesized superparamagnetic Fe_3O_4 nanoparticles showed that the catalyst activity decreased from 85% in the first cycle to 78% in the fifth cycle.

Silver chromate/reduced graphene oxide nanocomposites (Ag_2CrO_4/rGO NCs) with a narrow dissemination size were used for the removal of Methylene Blue [136]. The photodegradation of the dye was carried out under solar light irradiation. Experimental results indicated removal efficiencies of near 92% after one hour of irradiation, result which compared well with the results reached by pure Ag_2CrO_4 (46%) and rGO (30%) nanomaterials. The nanocomposites maintained their efficiency to degrade for up to five cycles.

The spherical shaped monoclinic structures, ZnO (24.9 nm) and CuO (17.0 nm) nanoparticles and ZnO/CuO (22.6 nm) nanocomposites were synthesized using extract of *Musa acuminate* fruit peel as the stabilizing and capping agent [137]. Degradation investigations on Methylene Blue had been carried out using these nanomaterials under a visible light source. ZnO, CuO, and ZnO/CuO showed degradation efficiencies of 57%, 50%, and 90%, respectively.

Polypyrrole (Ppy)-In_2O_3 nanoparticles hybrids were fabricated to leverage its superoxide radical decomposition for Methylene Blue degradation [138].

The nanoemulsion procedure was utilized to synthesize $Bi_xSn_{6-2x}S_y$ ($0.33 \leq x \leq 2.95$) photocatalysts with morphological structures that changed from nanowhiskers to quantum dots [139]. Particularly, $BiSn_4S_{4.5}$ formulation, photodegraded Methylene Blue in the shortest time under UV-visible light (Table 6).

Table 6. Percentage of degradation, under UV-visible light, of Methylene Blue using various $Bi_xSn_{6-2x}S_y$ formulations.

Material	0 hours	10 min	0.25 hours	1 hour	3 hours
SnS	0	no data	68	86	93
$Bi_{0.3}Sn_{5.34}S_{5.8}$	0	no data	43	50	82
$BiSn_4S_{5.5}$	0	100	100	100	100

From [139].

Copper oxide (CuO) was used to dope tin oxide (SnO_2) in order to yield a heterostructured photocatalyst, which were used in the degradation of Methylene Blue [140]. The oxides mixture degraded the dye with 90% efficiency in three hours, which improved the results derived with the use of SnO_2.

Black titanium dioxide (BTO) nanoparticles were formed, using pulsed laser irradiation in liquids, from de-ionized water, isopropyl alcohol, and 1:1 mixtures of water and alcohol [141].

 doi:10.20944/preprints202405.1122.v1

Photocatalytic degradation of Methylene Blue was improved at neutral pH values of the solution. This degradation occurred *via* reaction of the dye with ·OH, O_2^{-} and ·OOH radicals to produce CO_2 and water. The efficiency decay, for every adsorbent, approximately 10% after continuous use (three cycles), though for the four adsorbents tested, only BTOWA degraded the dye at 54% in the first cycle.

Ag-manganese oxide, with plasmon-enhanced photocatalytic activity, the photodegradation of Crystal Violet dye was formed. Manganese oxide was prepared by an acidic precipitation method using potassium permanganate, manganese acetate, and nitric acid as precursors. Silver nanoparticles were deposited on the manganese oxide using leaf extracts of *Calotropis gigantean* [142]. The deposition of silver increased the photocatalytic activity of the manganese oxide from 68 to 95%. By the use of 10% Ag-OMS, near 100, 95, and 75% efficiencies in the photodegradation of 50, 100, and 150 mg/L dye concentrations was observed in 90, 120, and 120 min, respectively. After three cycles of activity, the efficiency to degrade the dye was maintained above 90%.

Pristine and carboxylic acid (CXA)-modified MIL-53 (Al) nanostructures were used to investigate its performance on the adsorption of Rhodamine B and Methylene Blue from solutions [143]. The incorporation of the acidic function to MIL-53 (Al) produced an increase of the adsorption capacity, though Rhodamine B was adsorbed better than Methylene Blue due to its higher adsorption energy.

Cellulose acetate/polycaprolactone (CA/PCL)-based nanocomposites with manganese tungstate ($MnWO_4$) nanoparticles were formed, and used on the Crystal Violet photocatalytic degradation under UV light source [144]. The photocatalytic efficacy of the CA/PCL/$MnWO_4$ nanocomposites was higher to that of the individual components.

2D layered molybdenum disulphide/boron nitrate/reduced graphene oxide ($MoS_2$by/BN/rGO) ternary nanocomposites was formed by sonication assisted hydrothermal procedure, and its potential to treat water contaminated with Methylene Blue was investigated [145]. The nanocomposite ability to degrade the dye reached 98% after 45 min, with a ten percent loss of effectiveness, with respect to the first cycle, in the seventh cycle. The presence of superoxide radicals ($\cdot O_2^{-}$) and hydroxyl radicals ($\cdot OH^{-}$) were responsible for the degradation process.

TiO_2 nanotubes were annealed in the 400-900° C temperatures range to yield different nanomaterials and marked as TiO_2 ST-NT, moreover, part of these nanopowders were decorated with Fe_3O_4 nanoparticles to form TiO_2 ST-NT@Fe_3O_4NPs [146]. These nanocompounds were investigated for the photocatalytic decomposition of Methylene Blue under UV light. The best photocatalytic activity of TiO_2 ST-NT and TiO_2 ST-NT@Fe_3O_4NPs were yielded at annealing temperatures of 600 and 700° C, respectively.

Graphitic carbon nitride (g-C_3N_4) photocatalysts were prepared using mixtures of urea and thiourea, as precursors, by varying calcination temperatures ranging from 500 to 650° C for three hours in air medium, and used to remove Rhodamine B from liquid solutions [147]. The results showed that Rhodamine B removal by g-C_3N_4 formed at 600 °C was near 95% within three hours of visible LED light irradiation

$NiMn_2O_4$ nanoparticles had been prepared through PEG assisted hydrothermal method. This Ni4 nanosphere was used as a visible light photocatalyst for the degradation of Methylene Blue and Rhodamine B dyes [148]. Under optimized conditions and 210 min, the degradation rates of the two dyes were 68 and 80.7 %, respectively, whereas under five cycles of continuous use, the efficiency was maintained above 95% for both dyes.

Zinc oxide nanoparticles with spherical (40-100 nm) and rod (200 nm) shapes were fabricated using the extract from *Scallion peel*, and used to remove Methylene Blue presented in a mimic wastewater [149]. UV and visible light irradiation were used to degrade the dye. Experimental results showed that UV light was more effective (10 min) than visible light (30 min) to eliminate the dye from the solution.

Z-scheme V_2O_5/g-C_3N_4 photocatalytic composites were synthesized and used to degrade Methylene Blue [150]. This investigation showed that the optimum composite formulation had a 90% efficiency in the degradation of the dye, result which was near 6.18-fold higher than that of pristine

 doi:10.20944/preprints202405.1122.v1

GCN catalyst. After five cycles of continuous use, the GVO2 heterostructure showed a decrease in its degradation efficiency (from 90% in the first cycle to 80% in the fifth cycle).

Zn, and Fe co-doped TiO_2 photocatalyst were fabricated by the sol-gel method at room temperature, presenting the tetragonal anatase phase of TiO_2 in all synthesized nanoparticles [151]. Also, it was shown the presence of spherical nanoparticles in ZFT_2.5 photocatalyst with a diameter ranging from 8 to 20 nm. The photocatalyst ZFT_2.5 was investigated for the photocatalytic degradation of a mixture of three cationic dyes (Rhodamine B, Malachite Green and Methylene Blue) under exposure to visible light. Experimental results indicated that the above dyes degraded with 90.57%, 91.54% and 88.39%, respectively.

Graphite oxide and carbon quantum dots (CQDs) were added to polyacrylonitrile nanofibers to investigate its performance, under visible light irradiation, on the photocatalytic degradation of Methylene Blue. Quantitative degradation efficiency for the dye was found after 25 min, showing the nanocomposite better efficiency than the pristine precursors [152].

A green procedure was used to create MgO NPs using *Manilkara zapota* as a bio source, further, activated carbon/magnesium oxide (AC/MgO) photocatalyst was blended through a solution evaporation procedure [153]. This photocatalyst was used for photodegradation of Rhodamine B using an UV–visible spectrophotometer. The dye can be degraded (99%) under simulated solar irradiation.

Cadmium doped ZnO nanocomposites was prepared to investigate its performance on the photocatalytic degradation of Methylene Blue [154]. Cadmium doping in ZnO nanostructure acted as an electron scavenger, stopping electron-hole (e^-/h^+) pairs from recombination on the surface of ZnO and increasing charge transfer.

Pure and TiO_2 doped MnO_2 spherical nanoparticles were made using a sol-gel technique. These nanoparticles were investigated in the photocatalytic degradation, under visible light exposure, of Methylene Blue [155]. However, the use of the titanium-bearing nanomaterial only produced, after 120 min, a little improvement over the use of MnO_2. The utilization of both nanomaterials under continuous cycles indicated that there was a continuous loss of the activity after five cycles, being more displayed in the case of MnO_2 than in the TiO_2-MnO_2 material.

Titanium dioxide nanoparticles (spherical shape) were formed, using leaf extracts of a sausage tree (*Kigelia Africana*), and evaluated for the photocatalytic degradation of Toluidine Blue [156]. This nanomaterial removed the dye with a 99.6 % efficiency within one hour and under an UV–visible source.

A MoS_2/$FeMoO_4$ composite was formed by introducing MoS_2 (which actuate as inorganic promoter) into MIL-53(Fe)-derived PMS-activator [157]. The prepared MoS2/$FeMoO_4$ activated peroxymonosulfate (PMS) to reach 99.7% of Rhodamine B degradation after 20 min. Both Fe(II) and sulfur vacancies were responsibles as the main active sites on catalyst surface, where sulfur vacancies can promote adsorption and electron migration between PMS and MoS_2/$FeMoO_4$ to boost peroxide bond activation.

Rough copper oxide with a nanostructural morphology and located on the surface of a copper sheet was formed by an electrochemical anodic oxidation procedure; these nanostructures were used in the degradation of Rhodamine 6G under the irradiation of visible light [158].

Silver-doped borophene and the corresponding zero-dimensional boron were constructed [159]. They were used to investigate its performance on the photocatalytic degradation, under UV-visible irradiation, of Rhodamine B. The dye completely degraded after 120 min, though a small but continuous decrease in the efficiency after the 2nd and 3rd cycles was shown.

The same dye (Rhodamine B), than in the previous reference, was photocatalytic degraded by the action of Bi_2O_3@Zn-MOF hybrid nanomaterials, which were synthesized by supporting Zn-based metal-organic framework (Zn-MOF) through a hydrothermal process [160]. A catalytic efficiency of 97% was reached after 90 min of exposure to visible light irradiation. Generation of free radicals ($\cdot O_2^-$ and $\cdot OH$) was responsible for the decomposition of the dye into CO_2 and water. The nanocomposite can be reused three times, though the degradation efficiency decreased to 78 %.

 doi:10.20944/preprints202405.1122.v1

MnS_2/MnO_2-CC heterostructure dual-functional catalysts formed of ultrathin nanosheets were prepared by a two-step electrodeposition method for used in the degradation of Methylene Blue [161]. The dye removal efficiency of the heterostructural catalyst with a better kinetic rate (0.0226) can reach 97.76%, which is much higher than that of the MnO_x-CC catalyst (72.10%).

Based on the biopolymer pomelo peels (PP) and metal-oxide catalyst manganese oxide (MnO_x), an adsorption-enhanced catalyst (MnO_x-PP) was constructed for catalytic Methylene Blue oxidative-degradation [162]. The dye was adsorbed onto the biopolymer and then the continuous generation of active substances ($O_2^{\cdot}$ and $OH^{\cdot}$) degraded *via* an oxidative process the adsorbed dye molecules. Methylene Blue was degraded at a 99.5% rate at 25º C and one hour, with a slight (5%) but continuous dynamic degradation efficiency during 72 h based on the self-built continuous single-pass dye purification device.

3.4. Remarks to the Use of Nanomaterials in the Removal of Cationic Dyes from Solutions

In the case of cationic dyes, the use of (photo)-catalysis methodology surpass the utilization of adsorption-elution processes to remove these harmful dyes. A new approach, as being the formulation of nanomaterials-bearing mixed matrix membranes has been developed for the removal of cationic dyes (Methylene Blue) from a simulated wastewater. Similarly to the case of anionic dyes, it is extremely subjective, independently of the used methodology, to compare one nanomaterial from another due to the various experimental conditions used in the works. In the case of (photo)-catalytic approaches, times to degrade the very same dye varies from 10 min to 3 hours (Methylene Blue) or 12 min to 3 hours (Rhodamine B), whereas in the case of adsorption processing the dye uptakes also show a variety of numbers. Table 7 showed a list of dyes used in the various investigations. In the case of cationic dyes, Methylene Blue is the dye most investigated using any removal methodology. Table 8 summarized some results about efficiencies found in the removal of Methylene Blue or Rhodamine B using the (photo)-catalytic approach, it can be seen that efficiencies in the removal of these dyes ranged from a few minutes to hours. It is also worth to notice here that despite the good removal characteristics of the different nanomaterials, very few show significant stability under continuous use. Also, no one of these investigations used real wastewaters.

Table 7. Summary of methodologies and cationic dyes used in the investigations.

Methodology	Cationic dye	Reference
Adsorption	Crystal Violet	[97]
	Basic Fuchsin	[98]
	Golden Yellow, Methylene Blue	[99,101,103,105–108]
	Basic Red 114	[100]
	Malachite Green	[102,109]
	Methylene Blue, Methylene Violet, Brilliant Green	[103]
	Toluidine Blue O	[104]
	Rhodamine B	[107]
Membranes	Methylene Blue	[110]
(Photo)-catalysis	Methylene Blue	[111–113,115–120,123–127,130,132,136–141,143,145,146,149–155,161,162] [114,115,118,122,123,128–131,134,135,147,148,151,154,157,159,160]

 doi:10.20944/preprints202405.1122.v1

	Rhodamine B	[117,121,133,151]
		[121,123,142,144]
		[156]
	Malachite Green	[159]
	Crystal Violet	
	Toluidine B	
	Rhodamine 6G	

Table 8. (Photo)-catalytic removal of Methylene Blue and Rhodamine B.

Dye	Nanomaterial	Efficiency-time	Reference
Methylene Blue	$Mn_4(P_2O_7)$	99%-30 min	[113]
	Ce-Co,Fe ferrites	95%-1 hour	[116]
	La-Co,Fe,Ti composite	99%-50 min	[120]
	Fe_3O_4@APF@Ag	90%-3 min	[130]
	Mixed Fe,Mn,Cu oxides	95%-2.5 hours	[132]
	$AgCrO_4$-rGO	92%-1 hour	[136]
	CuO-SnO_2	90%-3 hours	[140]
	$NiMn_2O_4$	68%-3.5 hours	[148]
	CO-CQ dots	100%-25 min	[152]
Rhodamine B	Fe_3O_4@APF@Ag	90%-3 min	[130]
	AgO nanoparticles	76%-1 hour	[131]
	Fe_3O_4 nanoparticles	85%-12 min	[135]
	g-C_3N_4	95%-3 hours	[147]
	$NiMn_2O_4$	81%-3.5 hours	[148]
	Mo,Fe-sulphur-oxide	99.7%-20 min	[157]

4. Nanomaterials for the Removal of Anionic and Cationic Dyes

To mark some difference with the previous Sections in which nanomaterials were developed to remove anionic or cationic dyes, some scientists developed nanomaterials to be applied on the removal of both anionic and cationic dyes from solutions. This Section reviewed the performance of such nanomaterials with double use.

4.1. Adsorption of Anionic and Cationic Dyes on Nanomaterials

Black Liquors-based aerogels with Carbon Nanostructures (BL-CN), performance against dyes uptake, was compared with that of Carbon Nanostructures aerogels (CN) without the presence of Black Liquors [163]. Experimental results concluded that BL-CN aerogels presented better adsorption loadings of Methylene Blue and Brilliant Blue than those produced by CN-based aerogels: 256 mg/g (CN) versus 307 mg/g (BL-CN) for Methylene Blue, and 7 mg/g (CN) to 61 mg/g (BL-CN) for Brilliant Blue. BL-CN materials from pulping of RS with alkaline reagents (NaOH and KOH–NH_4OH) were the basis for the best Methylene Blue adsorbents, whereas best Brilliant Blue uptakes were obtained with BL-CN adsorbents from sulfite reagent.

Next reference [164], investigated the performance of biological graphene hydrogel (BGH) formed by *Shewanella putrefaciens* CN32 on the removal of Methyl Orange and Methylene Blue. Using BGHs and 24 hours of reaction time, removal efficiencies reached near 93% and 91%, for the respective anionic and cationic dye, increasing the efficiency with respect to the use of non-graphene materials. No data about the recyclability of the nanomaterial.

 doi:10.20944/preprints202405.1122.v1

Carbon dots/silica nanoaggregates for dye adsorption were synthesized via a hydrothermal reaction of N-doped carbon dots with (3-aminopropyl)triethoxysilane. With experimental data fitted to the Langmuir isotherm model, these nanoaggregates presented adsorption uptakes of 1327 mg/g for Alizarina Red S and 4091 mg/g for Malachite Green [165].

The next reference [166], presented a machine learning investigation about the adsorption of organic dyes onto nanozeolites and to conclude which variables influenced their adsorption uptake from wastewater. Four ML algorithms (Random Forest, Light Gradient Boosting, eXtreme Gradient Boosting, and Artificial Neutral Network) were tested as regression models, with XGB presenting the best usefulness in terms of prediction of the adsorption uptake of nanozeolite from a relatively small dataset. The data concluded that cationic dyes (Crystal Violet and Acridrine Orange) uptake (about 12 mg/g) are much better than that of anionic dyes (less than 0.5 mg/g) on these nanoadsorbents.

Cellulose was obtained, from coconut husk fiber, via an alkali-acid hydrolysis procedure with formation of nano-crystalline cellulose (NCC), presenting spherical shape with diameters below 40 nm [167]. NCC was investigated for its adsorption capacity against various dyes, being the removal efficiencies near 91% for Methylene Blue and 90% for Congo Red at all the pH values, with the adsorption of Crystal Violet reaching a maximum at pH 9, and the corresponding to Methyl Red at pH 5.

Spirulina-mediated titanium oxide nanoparticles (STONPs) were fabricated and used to investigate its performance on the adsorption of Methyl Orange and Malachite Green [168], and whereas Methyl Orange was best remove from the solution at pH 4, the pH value for the maximum Malachite Green removal was 12. The maximum uptake using the Langmuir isotherm model was 272.5 mg/g and 209.6 mg/g for the respective above dyes. There was a continuous and important lost of removal efficiency after five cycles.

4.2. Nanomaterials–Forming Membranes for the Removal of Anionic and Cationic Dyes

An MXene nanocomposite functionalized with a zwitterion (Z-MXene) was fabricated to be used as nanofiller in the development of self-cleaning permeable membranes [169]. The presence of functional groups and negative charge on the nanocomposite surface improved the separation of Congo Red and Methylene Blue by near 275 and 400%, respectively; at the same time, a high water flux was maintained. The composite membrane is chemically stable in the presence of corrosive (2 M HCl) and oxidative (NaOCl) media.

A polyacrylonitrile (PAN) electrospun membrane was build as scaffold to incorporate nanomaterial adsorbents in a layer-by-layer hierarchical structure [170]. Two different nanomaterials were incorporated: a positively charged metal organic framework as MIL-101(Cr), and negatively charged functionalized multi-walled carbon nanotubes; these were used to remove anionic (Methyl Orange and Rose Bengal) and cationic (Methylene Blue) dyes. Operating at 0.04 bar, removal efficiencies of the membrane incorporating MIL-101(Cr) were 5% (Methyl Orange) and 99% (Rose Bengal) from an iso-propylic alcohol medium. MWCNT-based membrane showed 90% removal of Methylene Blue also in the same alcoholic medium, and operating at 0.07 bar.

Graphene oxide–copper oxide (GO–CuO) nanomaterial had been incorporated into cellulose-acetate (CA) and poly-ether sulfone (PES) blend polymer by using phase inversion process to fabricate thin film nanocomposite (TFN) membranes, which were used on the removal of Methylene Blue, Rhodamine B, Methyl Orange and Congo Red [171]. In equilibrium conditions, the composite membrane removed 92%, 89%, 59% and 68% of the above respective dyes; thus, the TFN membrane seemed to be more effective to remove cationic dyes than anionic ones. The membrane was also used on the purification of a textile industry effluent sample (with no mention of the dyes contained in it), an all physio-chemical properties of the sample showed a decrease in their values when compared to the respective ones of the laboratory synthetic effluent.

Heterojunctions formed by UiO-66-NH2 and carbon quantum dots (CQDs) to investigate their synergetic advantages as nanofillers in thin-film nanocomposite (TFN) membranes for dye removal were utilized [172]. Comparing to the pristine thin-film composite membranes, the optimal TFN membranes embedded with 0.2 wt% UiO-66-NH_2/CQD improved pure water permeance by 89.7%

 doi:10.20944/preprints202405.1122.v1

and higher rejection of dyes of different charges and molecular weights (Methylene Blue, Methyl Blue, Methyl Orange and Direct Red 23). Moreover, the decrease of water flux caused by dye adsorption during the long-term filtration process can be recovered by 92–99% via photocatalytic degradation of the embebbed dyes within 10 min.

4.3.(Photo)-Catalytic Degradation of Anionic and Cationic Dyes Using Nanomaterials

A mesoporous rod-shaped ZnO/CuO/CeO_2 n-p-n heterojunction via a two-step co-precipitation technique was formed, to investigate its use on the degradation of Crystal Violet and Methyl Orange [173]. Under sunlight, the degradation efficiencies were 96% (Crystal Violet) and 88% (Methyl Orange), after 90 min of irradiation. The ultimate oxidizing species that degraded the dyes were O_2^- and •OH over photocatalyst under sunlight illumination. Also, the recycling experiments showed that the nanomaterial maintained its activity after three cycles.

Lanthanum and neodymium substituted cobalt–strontium (Co–Sr) spinel ferrite ($Co_{0.5}Sr_{0.5}RE_xFe_{2-x}O_4$, x= 0.00 and 0.06) catalysts were synthesized and used to degrade Congo Red and Rhodamine B dyes from an aqueous solution mixture [174]. It was determined that the energy bandgap ranged from 2.91 to 2.52 eV. The formulation in which x= 0.06 presented the greatest degradation rates for both dyes, being the ferrite containing Nd^{3+} the species presenting the highest rates of all (Table 9).

Table 9. Percentages of dyes degradation using various $Co_{0.5}Sr_{0.5}RE_xFe_{2-x}O_4$ formulations.

Nanomaterial	Congo Red	Rhodamine B
$Co_{0.5}Sr_{0.5}Fe_2O_4$	73	45
$Co_{0.5}Sr_{0.5}La_{0.06}Fe_{1.94}O_4$	81	67
$Co_{0.5}Sr_{0.5}Nd_{0.06}Fe_{1.94}O_4$	90	85

Time: One hour. From [174].

α-Fe_2O_3 was built at the nanometer (nanofibers) level *via* the electrospinning procedure to yield a nanomaterial with advanced characteristics to be used as photocatalysts to degrade Rhodamine B and Methyl Orange dyes [175]. The nanofibers fabricated from $FeCl_3{\cdot}6H_2O$ presented the best photocatalytic degradation, under visible-light irradiation, against the presence of both dyes in solution. The iron source is the key to yield a photocatalyst with the best degradation properties.

A solvothermal method was used to form mesoporous TiO_2, and (1-3 wt%) Cu-doped mesoporous TiO_2 membrane. Using artificial light source exposures, the effectiveness of the above materials on the degradation of Congo Red and Methylene Blue was investigated [176]. Cu-doping shifted the light absorption of mesoporous TiO_2 from the ultraviolet to the visible region. 3wt% Cu-doped mesoporousTiO_2 photocatalyst showed lower band gap energy (2.6eV) than TiO_2 (3.2 eV), thus, allowing the use of solar energy, and the exposure was shifted towards the visible region. Congo Red was degraded a 61% using mesoporous TiO_2 material, whereas the degradation reached 99% under the use of 3 wt% Cu-doped mesoporous TiO_2 material and pH of 5, in both cases the light exposure time was of 50 min. In the case of Methylene Blue, maximum degradation (95%) occurred at a pH value of 9.

It was investigated [177], the usage of Au/WO_3 composite as a photocatalyst for the degradation of dyes under solar light irradiation. Au/WO_3 nanocomposites (nanoplatelets and pseudospheres) were synthesized using an acid precipitation method followed by an impregnation/reduction at room temperature. The derived composites were formed with gold nanoparticles of 7 nm in size, whereas W(VI) was reduced to the W(V) oxidation state, and favouring the presence of oxygen vacancies and the presence of a surface plasmon resonance effect at 540 nm. At pH 5, the degradation produced with these Au/WO_3 photocatalysts was highly efficient on cationic dyes (Methylene Blue and Rhodamine B) rather than in Methyl Orange (anionic dye). Au/WO_3 forming pseudospheres, was the most efficient degrading material towards cationic dyes (near quantitative degradation at 60 min and 90 min for Rhodamine B and Methylene Blue, respectively). In the case of Methyl Orange, the gold-

 doi:10.20944/preprints202405.1122.v1

tungsten oxide was totally useless, at alkaline pH values, to degrade the dye, but at acidic pH values the degradation of the dye reached 80%.

Chitosan capped silver nanoparticles (Ag NPs-CS) adsorbents to remediate dye pollution had been photochemically formed under direct sunlight [178]. An aqueous Ag NPs-CS (100 μg/mL) degraded more than 95% of a mixed dye solution (25 mg/mL) containing equal volumes of Rhodamine B, Methylene Blue and Methyl Orange.

ZnO and Ag/ZnO nanocomposites were fabricated from *Basella alba* aqueous leaf extract. The Ag/ZnO nanocomposite showed degradation properties against the presence of Rhodamine B, Methylene Blue, and Methyl Orange, being the degradation efficiencies of 88%, 90%, and 92% for the respective dyes [179].

Copper-based organic@inorganic hybrid nanoflowers (Cu-hNFs) were obtained from *Tornabea scutellifera* lichen extract as the organic component [180]. Catalytic activity was show against Methylene Blue (maximum degradation effectiveness at pH 7.4) and Brillant Blue (best removed at pH 5). Both dyes degraded *via* a Fenton-like process.

α-MoO_3 nanoparticles synthesized by chemical co-precipitation were used as photocatalysts on the degradation of Methyl Orange and Methylene Blue under visible light exposure. Maximum degradation efficiencies reached 73% (anionic dye) and 95% (cationic dye) after 90 min [181].

Three commercially available ZnO powders were used for the tribocatalytic degradation of Rhodamine B, Methyl Violet, Methyl Blue and Methyl Orange dyes [182]. The removal of Rhodamine B reached near 99% efficiency after two hours, whereas after five hours of reaction time, the catalytic efficiencies in the removal of the separate dyes, followed the next order: Methyl Violet (99%)>Methyl Orange (85%)>Methyl Blue (55%). In the process, h+, $\cdot O_2^-$ and ·OH were generated, these radicals being responsible for the degradation of the respective dyes.

Bimetallic oxides were formed after the calcination of nanomaterials derived from metal-organic frameworks. When, Mn(M)-BTC nanomaterials was doped with Cu^{2+}, Fe^{2+}, Ce^{3+} or trimesic acid (H_3BTC), several derivatives were formed, being the material containing Cu^{2+}, the nanomaterial which presented the best degradation efficiency of several dyes: Methylene Blue, Rhodamine 6G, Eosin Y and Gentian Violet, in all these cases, the degradation efficiency was above 95% [183].

Semiconductor heterojunction systems of C-modified Zn-doped TiO_2 composite nanomaterials with nanofiber structures (150-200 nm diameter) were synthesized by electrospinning and hydrothermal methods [184]. Against the presence of Methylene Blue, Methyl Orange, Rhodamine B and Malachite Green, the composite nanofiber film had photocatalytic activity for all dyes attributable to the large specific surface area, small size effect and synergistic effects of multiple heterojunctions and dopant atom. The removal efficiency followed the Malachite Green>Methylene Blue>Methyl Orange>Rhodamine B order, being Methyl Orange efficiently removed with just 15 minutes.

Hybrid multifunctional nanoplexes composed of ZnS semiconductor quantum dots (ZnS QDs) chemically biofunctionalized with ε-poly-L-lysine (εPL), and coupled with magnetic iron oxide nanoparticles (MION, Fe_3O_4) stabilized by carboxymethylcellulose (CMC) were fabricated [185]. These nanoplexes were used to investigate its photocatalytic activity in the presence of Methylene Blue, Methyl Orange, Congo Red, and Rhodamine dyes. Degradation occurred *via* oxidation of the dyes by $\cdot O_2^-$ and ·OH radicals, and also by oxidation of dyes by holes:

$$ZnSQD(h^+_{VB}) + \text{dye} \rightarrow \text{degradation by} - \text{products} \quad (1)$$

In this investigation [186], ZnO nanoparticles (average size 15-30 nm) were synthesized by biosynthesis using dried *Peumus boldus* leaves. The photocatalytic activity of these nanomaterials indicated that it is possible the quantitative degradation of Methylene Blue in three hours, 92% in the case of Methyl Orange also in the same time, and 100% degradation of Rhodamine B in 30 minutes.

A n-type semiconductor as ZnO were coupled to a p-type one as CuO to form a p-n heterojunction. Further, the active surface of the heterojunction was increasedby addition of SiO_2-Aerogel [187]. By application of ultrasound, aerogel particles were better distributed, which the number of active sites were increased. CuO-ZnO/SA(P= 200) formulation (1 g/L) photocatalytically degraded 20 mg/L of each dye at pH 8: 95.4% in the case of Methylene Blue, whereas Methyl Orange

 doi:10.20944/preprints202405.1122.v1

degraded 56.1% and Congo Red until 71.3%. In the case of Methylene Blue, there was a continuous loss of efficiency after four cycles: 90.6% in the first cycle versus 78% in the fourth one.

Several materials such as, graphene oxide, magnetite-($FeO{\cdot}Fe_2O_3$), and hematite-(α-Fe_2O_3) decorated graphene oxide were investigated as Integrated Photocatalyst Adsorbents (IPCAs) in the oxidation of Methylene Blue, Crystal Violet and Tartrazine Yellow [188]. The cationic dyes showed maximum degradation, whereas the anionic dye presented acceptable removal rates when iron-decorated nanomaterials were used. In these cases, the efficiency order was: graphene oxide-αFe_2O_3>graphene oxide-Fe_3O_4>graphene oxide. All the nanomaterials maintained their photocatalytic activity for five cycles with dyes removal in the 86%-95% range.

Zinc selenide nanomaterials, produced from waste peels of orange and potato using the hydrothermal method, were utilized as photocatalysts to degrade Methylene Blue and Congo Red using sunlight [189]. Citrate in orange peel–mediated synthesis helped to form particle size of 1.85 nm and a surface area of 17.078 m^2/g, resulting in an increase of surface-active sites. These nanomaterials had a degradation efficiency of 97.16% and 93.61% for Methylene Blue and Congo Red, respectively.

Magnetic SiO_2 ($MagSiO_2$@PDA@MnO_2) were synthesized using magnetic, monodisperse-porous SiO_2 ($MagSiO_2$) as the starting material [190]. $MagSiO_2$@PDA@MnO_2 material was used to remove Rhodamine B, Methyl Orange and Methylene Blue, being the removal of the dyes attributable both, to physical adsorption and degradation *via* peroxymonosulfate activation. Removal efficiency followed ethylene Blue>Rhodamine B>Methyl Orange sequence, whereas the dyes removal rate showed that the degradation occurred *via*physical adsorption and peroxymonosulfate oxidation. After five cycles, there was a small decrease in the dyes removal efficiencies probably due a decrease in the manganese content of the material.

Silver nanoparticles (AgNPs) were synthesized from *Echinophora platyloba* plant extract, which acted as both reducing agent and capping agent in the synthesis of the nanoparticles [191]. It was found that pH played a key role in determining particle sizes, which can be tuned from 15 nm to 53 nm when the pH decreased from 10 to 7. AgNPs (15 nm) showed remarkable catalytic performance in degradation of different individual azo dyes (i.e. Methylene Blue (90.1%), Congo Red (80.1%), Rhodamine B (87.2%), Methyl Red (80.3%), Bromocresol Blue (92.5%) and Imido Black (79.8%)), as well as their mixture. It was found, that 79.2% of the mixture of dyes were decomposed in eleven minutes, following a pseudo-first order kinetic model.

Sunlight-active n–n heterojunction of TiO_2-coupled-CdS (TiO_2-CdS) was prepareded by using seed extract of *Sapindus mukorossi* and investigated in the removal of Rhodamine B and Congo Red [192]. The nanocomposite presented degradations of 93% and 95% for the above respective dyes, under the next experimental conditions: 25 mg/L dyes concentration, 15 mg of nanocomposite dosage, neutal pH and five hours of reaction time. Under continuous use (eight cycles of dye uptake and degradation), there was a continuous but slight efficiency lost in the treatment of both dyes, better displayed in the case of Rhodamine B than in Congo Red.

A solvothermal procedure converted electrical furnace slag into a steel slag nanocomposite (average particle size 34.8 nm), which were supported by H_2O_2 for Fenton and photo-Fenton-like degradation of various dyes in both suspension and spin-coated modes [193]. Using Methylene Blue and based on the optimum dye removal conditions (30 mg/L dye concentracion, pH 11, 1.59 mL/L H_2O_2 concentration, 58.1 mg/L nanocomposite dosage, and one hour) five cycles were carried out for suspension and spin-coated modes. In the fifth cycle, resulting data showed that 92.89% of dye degraded for suspension mode and 88.21% for spin-coated mode. At pH 7 and 30 mg/L of each dye, the photodegradation efficiency of Methylene Blue, Methyl Red, Rhodamine B, Congo Red, Acid Blue 25, and Methyl Orange depended largely on the type of dye, with cationic dyes removed more efficiently than anionic ones (Table 10).

Table 10. Efficiency in the removal of dyes with the steel slag nanocomposite.

Dye	% Efficiency
Methylene Blue	85.8

 doi:10.20944/preprints202405.1122.v1

Methyl Red	74.5
Rhodamine B	70.5
Congo Red	58.7
Acid Blue 25	45.2
Methyl Orange	40.4

Time: one hour. Neutral pH. From [193].

Different heterogeneous photocatalysts composed of highly reduced graphene oxide (HRG) and vanadium oxide (VO_x)-based nanocomposites (HRG-VOx) were formed (nanorods, nanosheets and urchins), and their photocatalytic activities to photodegrade Methylene Blue and Methyl Orange were investigated [194]. Among all the morphologies, nanocomposite consisting of urchin-shaped VO_x nanoparticles (HRG-VO_x-U) demonstrated superior photocatalytic properties towards the degradation of the dyes (99.1% for Methylene Blue after 45 minutes, and 97.2% for Methyl Orange after 35 minutes). After three cycles and under UV-light irradiation, there was a continuous lost in the efficiency of Methylene Blue degradation.

A supramolecular material (3-4 nm average particle diameter) formed by the hybridization of hydrophilic hydrazide-pillar[5]arene, as surface-modifier, and silver nanoparticles was used in the reduction of Methylene Blue, Rhodamine B, Rhodamine 6G, and Methyl Orange [195]. After five cycles of continuous use, the degradation efficiency was maintained almost constant in the case of Rhodamine B and Methyl Orange dyes, but suffered a continuous lost in the case of Rhodamine 6G (most notably) and Methylene blue.

ZnO nanoparticles (10 nm), as photocatalyst material, were used to degrade Remazol Brilliant Blue R and Brilliant Green [196]. Zinc acetate, sodium hydroxide, polyvinylpyrrolidone and ethylene glycol at 197° C formed the nanoparticles. After 90 min of reaction time, 500 ppm of ZnO degraded 73% and 51% of the respective above dyes.

MgO–ZnO (MZ) nanocomposite (nanoplates with 35-100 nm of thickness) was prepared by a co-precipitacion procedure with enhanced photodegradation properties under natural sunlight exposure [197]. Both cationic and anionic dyes were used in the degradation experiments, and it was found that both types of dyes completely degraded after 20 min of sunlight exposure. After five cycles of use, Rhodamine B, Methyl Orange, and Methylene Blue presented variations in their degradation efficiency: 96-91%, 91–85% and 98–92%, respectively.

Another nanomaterial, with photodegradation properties under sunlight exposure, to degrade cationic and anionic dyes, was used in the next investigation [198]. In this case, the material was a ZnO/CuO nanocomposite, with ZnO and CuO nanoparticles, and the cationic dyes were Methylene Blue and Rhodamine B, whereas Methyl Orange was the anionic dye used in the investigation. ZnO and CuO nanoparticles had been synthesized by a biosynthesis procedure using *Ficus benghalensis* leaf extract, whereas the nanocomposite was fabricated by the mortar pestle crushing/milling method. As it was somewhat expected, the efficiency of the nanocomposite to degrade the three dyes was higher than that yielded by the use of the single oxides. Using the nanocomposite during three hours and sunlight exposure, Methylene Blue degrades about 99%, against 80% of Rhodamine B and 67% of Methyl Orange.

Potato-on-rod-like Z-scheme plasmon Ag_2CrO_4–$Ag_2Mo_2O_7$ heterojunction nano-photocatalyst was synthesized by precipitation method to photodegrade different organic dyes under artificial sunlight [199]. Under the best experimental conditions of 0.1 g dose of (3:1) nanophotocatalyst, 10 mg/L dyes concentration and 90 minutes of exposure to light, the above nanophotocatalyst formulation exhibited the greatest efficiency in the photodegradation of 2-Naphthol Orange (97.8%), Rhodamine B (99.7%), Crystal Violet (98.9%), and Methyl Orange (56.1%). In the case of 2-Naphtol Orange, the 3:1 catalyst formulation showed an acceptable reusability since the dye adsorption ran from 97.8% (1st cycle) to 95.7% in the fourth cycle.

One-step hydrothermal procedure were used to form $Bi_2O_{2.33}$//Bi_2O_3@ECNF (electrospun carbon nanofibers), which combines both adsorption and photocatalytic performance. The nanocomposite

 doi:10.20944/preprints202405.1122.v1

removed 95% of Methyl Orange and 83% of Rhodamine B after 2 and 3 hours, respectively. Both h^+ and ·OH were the main active species in the photocatalytic process under light exposure [200].

4.4. Remarks to the Use of Nanomaterials in the Removal of Anionic and Cationic Dyes from Solutions

At a first instance, the uses of these nanomaterials have the advantage, over the utilization of nanomaterials with a single use, that they are triggered with a broad scope since they are useful to remove anionic as well as cationic dyes from solutions. However, they present somewhat the same negative characteristics than the others, especially to that refereed to their stability under continuous cycle, when this data are shown in the published manuscript, because in many of the reviewed references, authors did not mention this issue about their respective investigated nanomaterial. As in previous cases, comparison between the different nanomaterials is subjective due to the different experimental conditions, and in this case another variable must be considered: the different mixtures of dyes used in the investigations. As it is previously done, Table 11 summarized the methodologies used to remove the mixture of anionic and cationic dyes.

Table 11. Summary of methodologies and anionic and cationic dyes used in the investigations.

Methodology	Dyes	Reference
Adsorption	Methylene Blue, Brilliant Blue	[163]
	Methyl Orange, Methylene Blue	[164] `
	Alizarin Red S, Malachite Green	[165]
	Crystal Violet, Acridine Orange	[166]
	MB.CR,CV,MR	[167]
	Methyl Orange, Malachite Green	[168]
	Congo Red, Methylene Blue	[169]
Membranes	MO,RB,MB	[170]
	MB,RhB,MO,CR	[171]
	MB,MeB,MO	[172]
(Photo)-catalysis	Crystal Violet, Methyl Orange	[173]
	Congo Red, Rhodamine B	[174,192]
	Rhodamine B, Methyl Orange	[175]
	Congo Red, Methylene Blue	[176,189]
	MB,RhB,MO	[177,178,186,190,197,198]
	Methylene Blue, Methyl Orange	[179,181,194]
	Methylene Blue, Brilliant Blue	[180]
	RhB,MV,MeB,MO	[182]
	MB,RhB,EY,GV	[183]
	MB,MO,RhB,MG	[184]
	MB,MO,CR,RhB	[185]
	MB,MO,CR	[187]
	MB,CV,TY	[188]
	MB,CR,RhB,MeR	[191]
	MB,MeR,RhB,CR,AB25,MO	[193]

 doi:10.20944/preprints202405.1122.v1

MB,RhB,Rh6G,MO	[195]
RBBR,BG	[196]
NO,RhB,CV,MO	[199]
Methyl Orange, Rhodamine B	[200]

AB25: Acid Blue 25. BG: Brilliant Green. CR: Congo Red. CV: Crystal Violet. EY: Eosin Y. GV: Gentian Violet. MB: Methylene Blue. MeB: Methyl Blue. MeR: Methyl Red. MG: Malachite Green. MO: Methyl Orange MR: Methyl Red. MV. Methyl Violet. NO: Napthol Orange. RBBR: Ramazol Brillian Blue R. RhB: Rhodamine B. Rh6G: Rhodamine 6G. RS: Rose Bengal. TY: Tartarzine yellow.

As an example of what it is mentioned above, using the same mixture (Methylene Blue, Rhodamine B and Methyl Orange) of dyes, results indicated that in [197] complete degradation of the dyes occurred after 20 min, against efficiencies of 99% (Methylene Blue), 80% (Rhodamine B) or 67% (Methyl Orange) in 3 hours declared in [198]. These last results hardly compared with data from [186], in which is demonstrated that Rhodamine B is completely eliminated after 30 min. Another mixture of dyes (Methylene Blue and Methyl Orange) show the same disparity in results, since 90 min are needed to remove 95% and 75% of the respective cationic and anionic dye [181], and 45 min (99% Methylene Blue) or 35 min (97% Methyl Orange) as concluded in [194].

Conclusions

This review emphasized the importance that the removal or organic dyes from solutions have on the scientific community; in this removal, two approaches are followed: adsorption or catalytic-photocatalytic degradation of the dye, whereas the use of nanomaterials is of widespread use.

In the case of adsorption methodology, all the references reviewed but two fitted its experimental data to the Langmuir isotherm model, the two exceptions are references [102] and [109] which fitted its data to the Freundlich isotherm. However, these nanomaterials performed quite different in the removal of both cationic and anionic dyes, and within the very same dye, as results in Table 12 demonstrated in the case of the adsorption of Congo Red and Methylene Blue. In the case of the anionic dye, maximum loadings vary from a few mg/g to the g/g magnitude order, whereas in the case of Methylene Blue the tendency is the same. These variations can be generalized to other dyes.

Table 12. Some maximum capacities of dyes on nanomaterials. .

Congo Red, mg/g	Reference	Methylene Blue, mg/g	Reference
17.8	[56]	5.78	[118]
47.4	[51]	36.4	[166]
57.8	[57]	332	[105]
3017	[60]	477	[108]
4334	[63]	736	[101]
8300	[62]		

With these results, it is amazing that some authors expressed their data as 8300 mg/g instead of the more logical 8.3 g/g form.

In the utilization of (photo)-catalytic methodology the results have the same tendency as those showed in Table 12 and commented in subsection 2.3. (Table 5), subsection 3.4. (Table 8) and text on subsection 4.4. The efficient in the removal of a given anionic or cationic dye is reached after minutes or several hours depending of the nanomaterial used. In the opinion of the present authors, other

 doi:10.20944/preprints202405.1122.v1

considerations (see below) may be taking into account prior to select one or another nanomaterial for each specific use or the methodology used to carry out this removal.

A point to consider is the tendency that some authors provided data with *little* scientific sense, as it is exemplified with the values of the thermodynamic data calculated from selected references (Table 13).

Table 13. Some *strange* thermodynamic values taken from the literature.

ΔH◦, kJ/mol	ΔS◦	Reference
-3.1689	-0.0112 J/K·mol	[101]
54.996	0.283 kJ/K·mol	[105]
3.568	0.0278 kJ/K·mol	[108]
7.09731	40.4502 J/K·mol	[168]

As it is seen, values are given within three-four decimals which does not correspond with the accuracy of the methodology used to calculate such numbers, also the responsibility to publish such values is not only of the authors but also of the respective reviewers (and Editors) allowing to do this.

Since the removal of dyes from solutions is of the utmost interest, future trends may be focused in: i) the development of more stable nanomaterials to be used in cycles (a general rule observed in this review is that there is a loss of efficiency with continuous cycles), ii) investigations of the use of nanomaterials on real dye-bearing wastes (in this review just only two, [58] and [171], references use industrial wastewaters in the investigation, iii) the use of dynamic conditions (columns) in the removal of dyes, and iv) a reliable knowledge about the easiness and costs to fabricate the nanomaterials in a greater scales than laboratory one. All the above will be key-points to understand the performance of the nanomaterials in the selected technology under long-term use.

References

1. Afshari, M.; Varma, R.S.; Saghanezhad, S.J. Catalytic applications of heteropoly acid-supported nanomaterials in synthetic transformations and environmental remediation. *Comments Inorg. Chem.* **2023,** *43,* 129–176. DOI: 10.1080/02603594.2022.2109019
2. Ansari, A.A.; Shamim, M.A.; Khan, A.M.; Anwar, K.; Wani, A.A. Nanomaterials as a cutting edge in the removal of toxic contaminants from water. *Mater. Chem. Phys.* **2023,** *295,* 127092. DOI: 10.1016/j.matchemphys.2022.127092
3. Bhattu, M.; Singh, J. Recent advances in nanomaterials based sustainable approaches for mitigation of emerging organic pollutants. *Chemosphere* **2023,** *321,* 138072. DOI: 10.1016/j.chemosphere.2023.138072
4. Mathew, A.T.; Saravanakumar M.P. Remediation of endocrine disrupting compounds and organic dye pollutants through biosorbents in a circular bioeconomy: prospects and constraints. *Environ. Sci. Eng.* **2023,** *F272,* 163–175. DOI: 10.1007/978-3-031-29597-3_14
5. Orimolade, B.O.; Idris, A.O.; Akanji, S.P.; Adekola, F.A.; Azizi, S.; Maaza, M.; Mamba, B. Solar-light-responsive nanomaterials for the photoelectrocatalytic degradation of stubborn pollutants. *Coatings* **2023,** *13,* 159. DOI: 10.3390/coatings13010159
6. Rajabi, M.; Keihankhadiv, S.S.; Tyagi, I.; Karri, R.R.; Chaudhary, M.; Mubarak, N.M.; Chaudhary, S.; Kumar, P.; Singh, P. Comparison and interpretation of isotherm models for the adsorption of dyes, proteins, antibiotics, pesticides and heavy metal ions on different nanomaterials and non-nano materials—a comprehensive review. *J. Nano. Chem.* **2023,** *13,* 43-65. DOI: 10.1007/s40097-022-00509-x
7. Monteiro, Lívia G.; Figueiredo, Marco A.G. Technology roadmap: nanomaterials applied to the tertiary treatment of industrial wastewater contaminated by synthetic organic dyes. *Chem. Eng. Trans.* **2023,** *101,* 1–6. DOI: 10.3303/CET23101001
8. Ponce, S.; Murillo, H.A.; Alexis, F.; Alvarez-Barreto, J.; Mora, J.R. Green synthesis of nanoparticles mediated by deep eutectic solvents and their applications in water treatment. *Sustainability* **2023,** *15,* 9703. DOI: 10.3390/su15129703

 doi:10.20944/preprints202405.1122.v1

9. Aswini, R.; Padmanaban, A.; Vigneshwaran, S.; Valdes, H.; Arunachalam, S.V. A review on versatile nano-photocatalysts for environmental remediation: carbon-decorated bismuth-based nanomaterials. *Nano-Struct. Nano-Objects* **2023,** *35,* 100991. DOI: 10.1016/j.nanoso.2023.100991
10. Oladipo, A.A.; Mustafa, F.S. Bismuth-based nanostructured photocatalysts for the remediation of antibiotics and organic dyes. *Beilstein J. Nanotechnol.* **2023,** *14,* 291–321. DOI: 10.3762/BJNANO.14.26
11. Linghu, X.; Shu, Y.; Liu, L.; Zhao, Y.; Zhang, J.; Chen, Z.; Shan, D.; Wang, B. Hydro/solvothermally synthesized bismuth tungstate nanocatalysts for enhanced photocatalytic degradation of dyes, antibiotics, and bacteria in wastewater: a review. *J. Water Proc. Eng.* **2023,** *54,* 103994. DOI: 10.1016/j.jwpe.2023.103994
12. Bairamis, F.; Rapti, I.; Konstantinou, I. g-C_3N_4 based Z-scheme photocatalysts for environmental pollutants removal. *Curr. Opin. Green Sust. Chem.* **2023,** *40,* 100749. DOI: 10.1016/j.cogsc.2022.100749
13. Umekar, M.S.; Bhusari, G.S.; Bhoyar, T.; Devthade, V.; Kapgate, B.P.; Potbhare, A.P.; Chaudhary, R.G.; Abdala, A.A. Graphitic carbon nitride-based photocatalysts for environmental remediation of organic pollutants. *Curr. Nanosci.* **2023,** *19,* 148–169. DOI: 10.2174/1573413718666220127123935
14. Bashir, M.; Batool, M.; Arif, N.; Tayyab, M.; Zeng, Y.-J.; Nadeem Z.M. Strontium-based nanomaterials for the removal of organic/inorganic contaminants from water: a review. *Coord. Chem. Rev.* **2023,** *492,* 215286. DOI: 10.1016/j.ccr.2023.215286
15. Bichave, M.S.; Kature, A.Y.; Koranne, S.V.; Shinde, R.S.; Gongle, A.S.; Choudhari, V.P.; Topare, N.S.; Raut-Jadhav, S.; Bokil, S.A. Nano-metal oxides-activated carbons for dyes removal: a review. *Mater. Today: Proc.* **2023,** *77,* 19-30. DOI: 10.1016/j.matpr.2022.08.451
16. Brillas, E.; Garcia-Segura, S. Recent progress of applied TiO_2 photoelectrocatalysis for the degradation of organic pollutants in wastewaters. *J. Environ. Chem. Eng.* **2023,** *11,* 109635. DOI: 10.1016/j.jece.2023.109635
17. Kanakaraju, D.; Chandrasekaran, A. Recent advances in TiO_2/ZnS-based binary and ternary photocatalysts for the degradation of organic pollutants. *Sci. Tot. Environ.* **2023,** *868,* 161525. DOI: 10.1016/j.scitotenv.2023.161525
18. Puri, N.; Gupta, A. Water remediation using titanium and zinc oxide nanomaterials through disinfection and photo catalysis process: a review. *Environ. Res.* **2023,** *227,* 115786. DOI: 10.1016/j.envres.2023.115786
19. Arun, J.; Nachiappan S.; Rangarajan, G.; Alagappan, R.P.; Gopinath K.P.; Lichtfouse, E. Synthesis and application of titanium dioxide photocatalysis for energy, decontamination and viral disinfection: a review. *Environ. Chem. Lett.* **2023,** *21,* 339-362. DOI: 10.1007/s10311-022-01503-z
20. Fan, Y.; Bai, Z.; Ge, Q.; Jiang, N.; Liu, M.; Cong, H.; Zhang, Y. Synergetic photodegradation via inorganic–organic hybridization strategies: a review on preparations and applications of nanoparticle-hybridized polyaniline photocatalysts. *J. Polym. Res.* **2023,** *30,* 8. DOI: 10.1007/s10965-022-03390-y
21. Farhan, A.; Arshad, J.; Rashid, E.U.; Ahmad, H.; Nawaz, S.; Munawar, J.; Zdarta, J.; Jesionowski, T.; Bilal, M. Metal ferrites-based nanocomposites and nanohybrids for photocatalytic water treatment and electrocatalytic water splitting. *Chemosphere* **2023,** *310,* 136835. DOI: 10.1016/j.chemosphere.2022.136835
22. Gusain, R.; Kumar, N.; Ray, S.S. Applications of MoS_2 nanostructures in wastewater treatment. *Springer Ser. Mater. Sci.* **2023,** *332,* 351–374. DOI: 10.1007/978-3-031-28756-5_12
23. Gadore, V.; Mishra, S.R.; Ahmaruzzaman, Md. Metal sulphides and their heterojunctions for photocatalytic degradation of organic dyes-a comprehensive review. *Environ. Sci. Poll. Res.* **2023,** *30,* 90410-90457. DOI: 10.1007/s11356-023-28753-w
24. Hani, U. Comprehensive review of polymeric nanocomposite membranes application for water treatment. *Alexandria Eng. J.* **2023,** *72,* 307-321. DOI: 10.1016/j.aej.2023.04.008
25. Suresh R.; Rajendran, S.; Gnanasekaran, L.; Show, P.L.; Chen, W.-H.; Soto-Moscoso, M. Modified poly(vinylidene fluoride) nanomembranes for dye removal from water–a review. *Chemosphere* **2023,** *322,* 138152. DOI: 10.1016/j.chemosphere.2023.138152
26. Hosny, N.M.; Gomaa, I.; Elmahgary, M.G. Adsorption of polluted dyes from water by transition metal oxides: a review. *Appl. Surf. Sci. Adv.* **2023,** *15,* 100395. DOI: 10.1016/j.apsadv.2023.100395
27. Saharan, P.; Kumar, V.; Kaushal, I.; Mittal, A.; Shukla, S.K.; Kumar, D.; Sharma, A.K.; Om, H. A comprehensive review on the metal-based green valorized nanocomposite for the remediation of emerging colored organic waste. *Environ. Sci. Poll. Res.* **2023,** *30,* 45677-45700. DOI: 10.1007/s11356-023-25998-3
28. Shanaah, H.H.; Alzaimoor, E.F.H.; Rashdan, S.; Abdalhafith, A.A.; Kamel, A.H. Photocatalytic degradation and adsorptive removal of emerging organic pesticides using metal oxide and their composites: recent trends and future perspectives. *Sustainability* **2023,** *15,* 7336. DOI: 10.3390/su15097336

29. Umar, E.; Ikram, M.; Haider, J.; Nabgan, W.; Imran, M.; Nazir, G. A state-of-art review of the metal oxide-based nanomaterials effect on photocatalytic degradation of malachite green dyes and a bibliometric analysis. *Global Chall.* **2023,** *7,* 2300001. DOI: 10.1002/gch2.202300001
30. Ali, J. Bibi, S.; Jatoi, W.B.; Tuzen, M.; Jakhrani, M.A.; Feng, X.; Saleh, T.A. Green synthesized zinc oxide nanostructures and their applications in dye-sensitized solar cells and photocatalysis: a review. *Mater. Today Comm.* **2023,** *36,* 106840. DOI: 10.1016/j.mtcomm.2023.106840
31. Leão, M.B.; Bordin, J.R.; de Matos, C.F. Specific surface area versus adsorptive capacity: an application view of 3D graphene-based materials for the removal of emerging water pollutants. *Water Air Soil Poll.* **2023,** *234,* 136. DOI: 10.1007/s11270-023-06146-6
32. Ojha, A.; Samriti; Thakur, S.; Prakash, J. Graphene family nanomaterials as emerging sole layered nanomaterials for wastewater treatment: recent developments, potential hazards, prevention and future prospects. *Environ. Adv.* **2023,** *13,* 100402. DOI: 10.1016/j.envadv.2023.100402
33. Prasad, C.; Madkhali, N.; Jeong, S.-G.; Malkappa, K.; Choi, H.Y.; Govinda V. Recent advances in the hybridization of cellulose and semiconductors: design, fabrication and emerging multidimensional applications: a review. *Int. J. Biol. Macromol.* **2023,** *233,* 123551. DOI: 10.1016/j.ijbiomac.2023.123551
34. Zhang, Y.; Zhang, Y.; Xu, W.; Wu, H.; Shao, Y.; Han, X.; Zhou, M.; Gu, P.; Li, Z. Preparation methods of cellulose nanocrystal and its application in treatment of environmental pollution: a mini-review. *Colloids Interface Sci. Comm.* **2023,** *53,* 100707. DOI: 10.1016/j.colcom.2023.100707
35. Li, S.; He, G.; Huang, J. Self-assembly on natural cellulose: towards high-efficient catalysts. *Curr. Opin. Colloid Interface Sci.* **2023,** *63,* 101655. DOI: 10.1016/j.cocis.2022.101655
36. Shahid-ul-Islam; Bairagi, S.; Kamali, M.R. Review on green biomass-synthesized metallic nanoparticles and composites and their photocatalytic water purification applications: progress and perspectives. *Chem. Eng. J. Adv.* **2023,** *14,* 100460. DOI: 10.1016/j.ceja.2023.100460
37. Singh, R.; Umapathi, A.; Patel, G.; Patra, C.; Malik, U.; Bhargava, S.K.; Daima, H.K. Nanozyme-based pollutant sensing and environmental treatment: trends, challenges, and perspectives. *Sci. Tot. Environ.* **2023,** *854,* 158771. DOI: 10.1016/j.scitotenv.2022.158771
38. Suresh R.; Rajendran, S.; Khoo, K.S.; Soto-Moscoso, M. Enzyme immobilized nanomaterials: an electrochemical bio-sensing and biocatalytic degradation properties toward organic pollutants. *Top. Catal.* **2023,** *66,* 691-706. DOI: 10.1007/s11244-022-01760-w
39. Wang, M.; Zhu, P.; Liu, S.; Chen, Y.; Liang, D.; Liu, Y.; Chen, W.; Du, L.; Wu, C. Application of nanozymes in environmental monitoring, management, and protection. *Biosensors* **2023,** *13,* 314. DOI: 10.3390/bios13030314
40. Yang, T.; Liu, X.; Zeng, Z.; Wang, X.; Zhang, P.; Feng, B.; Tian, K.; Qing, T. Efficient and recyclable degradation of organic dye pollutants by CeO_2@ZIF-8 nanozyme-based non-photocatalytic system. *Environ. Poll.* **2023,** *316,* 120643. DOI: 10.1016/j.envpol.2022.120643
41. Solangi, N.H.; Karri, R.R.; Mubarak, N.M.; Mazari, S.A.; Jatoi, A.S.; Koduru, J.R. Emerging 2D MXene-based adsorbents for hazardous pollutants removal. *Desalination* **2023,** *549,* 116314. DOI: 10.1016/j.desal.2022.116314
42. Chinnasamy, C.; Perumal, N.; Choubey, A.; Rajendran, S. Recent advancements in MXene-based nanocomposites as photocatalysts for hazardous pollutant degradation-a review. *Environ. Res.* **2023,** *233,* 116459. DOI: 10.1016/j.envres.2023.116459
43. Massoumılari, Ş.; Velioğlu, S. Can MXene be the effective nanomaterial family for the membrane and adsorption technologies to reach a sustainable green world?. *ACS Omega* **2023.** DOI: 10.1021/acsomega.3c01182
44. Zhang, Q.; Jia, Y.; Wu, W.; Pei, C.; Zhu, G.; Wu, Z.; Zhang, L.; Fan, W.; Wu, Z. Review on strategies toward efficient piezocatalysis of $BaTiO_3$ nanomaterials for wastewater treatment through harvesting vibration energy. *Nano Energy* **2023,** *113,* 108507. DOI: 10.1016/j.nanoen.2023.108507
45. Ahmadian, M.; Derakhshankhah, H.; Jaymand, M. Biosorptive removal of organic dyes using natural gums-based materials: a comprehensive review. *J. Ind. Eng. Chem.* **2023,** *124,* 102-131. DOI: 10.1016/j.jiec.2023.05.002
46. Chelu, M.; Musuc, A.M.; Popa, M.; Calderon Moreno, J.M. Chitosan hydrogels for water purification applications. *Gels* **2023,** *9,* 664. DOI: 10.3390/gels9080664

47. Ingrassia, E.B.; Lemos, E.S.; Escudero, L.B. Treatment of textile wastewater using carbon-based nanomaterials as adsorbents: a review. *Environ. Sci. Poll. Res.* **2023,** *30,* 91649-91675. DOI: 10.1007/s11356-023-28908-9
48. Jha, S.; Gaur, R.; Shahabuddin, S.; Tyagi, I. Biochar as sustainable alternative and green adsorbent for the remediation of noxious pollutants: a comprehensive review. *Toxics* **2023,** *11,* 117. DOI: 10.3390/toxics11020117
49. Amrhar, O.; Lee, H.-S.; Lgaz, H.; Berisha, A.; Ebenso, E.E.; Cho, Y. Computational insights into the adsorption mechanisms of anionic dyes on the rutile TiO_2 (1 1 0) surface: combining SCC-DFT tight binding with quantum chemical and molecular dynamics simulations. *J. Mol. Liq.* **2023,** *377,* 121554. DOI: 10.1016/j.molliq.2023.121554
50. Aydin Urucu, O.; Denïz, S.; Kahraman, N.; Çakmakçi, E. Itaconic acid-derived reactive protic ionic liquid (PIL)-containing superabsorbent green hydrogel adsorbent for the removal of anionic textile dyes. *Mater. Tod. Commun.* **2023,** *36,* 106867. DOI: 10.1016/j.mtcomm.2023.106867
51. Chen, X.; Chen, Y.; Zhang, L.; Liu, Z.; Qiu, E.; Liu, Q.; Regulacio, M.D.; Lin, C.; Yang, D.-P. Hydrophilic ZnO/C nanocomposites with superior adsorption, photocatalytic, and photo-enhanced antibacterial properties for synergistic water purification. *J. Coll. Interf. Sci.* **2023,** *648,* 535-550. DOI: 10.1016/j.jcis.2023.06.019
52.] Deniz, Sabahattin. Efficient and environmentally friendly removal of azo textile dye using a low-cost adsorbent: Kinetic and reuse studies with application to textile effluent. *Mater. Tod. Commun.* **2023,** *35,* 106433. DOI: 10.1016/j.mtcomm.2023.106433
53. Eizi, R.; Bastami, T.R.; Mahmoudi, V.; Ayati, A.; Babaei, H. Facile ultrasound-assisted synthesis of CuFe-Layered double hydroxides/g-C_3N_4 nanocomposite for alizarin red S sono-sorption. *J. Taiwan Inst. Chem. Eng.* **2023,** *145,* 104844. DOI: 10.1016/j.jtice.2023.104844
54. Hai, D.T.; Phuong, N.T.; Cong, P.X.; Nam, N.H.; Thu, L.P.; Trang, N.T.T.; Thom, N.T.; Nam, P.T.; Osial, M.; Thanh, D.T.M. Hydroxyapatite/superparamagnetic iron oxide nanoparticles nanocomposite for Congo Red adsorption. *Desalin. Water Treat.* **2023,** *298,* 184-198. DOI: 10.5004/dwt.2023.29630
55. Karyab, H.; Ghasemi, M.; Ghotbinia, F.; Nazeri, N. Efficiency of chitosan nanoparticle with polyaluminum chloride in dye removal from aqueous solutions: optimization through response surface methodology (RSM) and central composite design (CCD). *Int. J. Biol. Macromol.* ***2023,*** *249,* 125977. DOI: 10.1016/j.ijbiomac.2023.125977
56. Laxmi Deepak Bhatlu, M.; Athira P.S.; Jayan, N.; Barik, D.; Dennison, M.S. Preparation of breadfruit leaf biochar for the application of Congo Red dye removal from aqueous solution and optimization of factors by RSM-BBD. *Adsorp. Sci. Technol.* **2023,** *2023,* 7369027. DOI: 10.1155/2023/7369027
57. Mahmoud, M.E.; Moneim El-Ghanam, A.; Saad, S.R. Fast and efficient adsorptive capture of Congo red and Erythromycin pollutants by a novel nanobiosorbent from crosslinked nanosilica with nanobiochar and chitosan. *Inorg. Chem. Commun.* **2023,** *158,* 111557. DOI: 10.1016/j.inoche.2023.111557
58. Patil, D.J.; Behera, S.N. Synthesizing nanoparticles of zinc and copper ferrites and examining their potential to remove various organic dyes through comparative studies of kinetics, isotherms, and thermodynamics. *Environ. Monit. Assess*. **2023,** *195,* 591. DOI: 10.1007/s10661-023-11177-x
59. Qi, C.; Zhao, M.; Fang, T.; Zhu, Y.; Wang, P.; Xie, A.; Shen, Y. Multifunctional hollow porous Fe3O4@N-C nanocomposites as anodes of lithium-ion battery, adsorbents and surface-enhanced Raman scattering substrates. *Molecules* **2023,** *28,* 5183. DOI: 10.3390/molecules28135183
60. Qin, Z.; Dong, K.; Zhang, Y.; Jiang, Y.; Mo, L.; Xiao, S. Noval green sodium alginate/gellan gum aerogel with 3D hierarchical porous structure for highly efficient and selective removal of Congo red from water. *Biores. Technol.* **2023,** *370,* 128576. DOI: 10.1016/j.biortech.2023.128576
61. Rubangakene, N.O.; Elwardany, A.; Fujii, M.; Sekiguchi H.; Elkady, M.; Shokry, H. Biosorption of Congo Red dye from aqueous solutions using pristine biochar and ZnO biochar from green pea peels. *Chem. Eng. Res. Des.* **2023,** *189,* 636-651. DOI: 10.1016/j.cherd.2022.12.003
62. Vuong, N.-M.-T.; Nguyen, P.-T.; Nguyen, T.K.O.; Nguyen, D.B.; Tran, T.-M.-D.; Oanh, L.T.K.; Nguyen, T.-B.; Pham, T.-T.; Lin, K.-Y.A.; Bui, X.-T. Application of nano zero-valent iron particles coated by carboxymethyl cellulose for removal of Congo red dye in aqueous solution. *Case Stud. Chem. Environ. Eng.* **2023,** *8,* 100469. DOI: 10.1016/j.cscee.2023.100469

63. Zhu, R.; Zhang, L.; Zhang, Y.; Zhang, P.; Jia, Y.; Cheng, Q.; Wu, W.; Li, J. Two-dimensional acetate-based light lanthanide fluoride nanomaterials: An ultrahigh adsorption capacity and salt-tolerance endowed by surface acetates exchange. *Appl. Surf. Sci.* **2023,** *621,* 156842. DOI: 10.1016/j.apsusc.2023.156842
64. Aaga, G.F.; Anshebo, S.T. Green synthesis of highly efficient and stable copper oxide nanoparticles using an aqueous seed extract of Moringa stenopetala for sunlight-assisted catalytic degradation of Congo red and Alizarin red S. *Heliyon* **2023,** 9, e16067. DOI: 10.1016/j.heliyon.2023.e16067
65. Afaq, M.; Basha, B.; Warsi, M.F.; Shahid, M.; Alrowaili Z.A.; Al-Buriahi M.S.; Yousaf, S. Fabrication of ZnO-CuFe2O4-CNTs ternary nanocomposite for harmful organic effluents degradation by sunlight irradiation. *Mater. Sci. Eng. B Solid State Mater. Adv. Technol.* **2023,** *292,* 116444. DOI: 10.1016/j.mseb.2023.116444
66. Ashfaq, M.; Ali, A.; Abbood, N.K.; Panchal, S.; Akram, N.; Saeed, M.; Doshi, O.P.; Ali, F.; Muhammad, S., Sameeh, M.Y.; Nazar, A.N. Enhanced photocatalytic activity of the Bi_2O_3-NiO heterojunction for the degradation of methyl orange under irradiation of sunlight. Water **2023,** *15,* 3182. DOI: 10.3390/w15183182
67. Barhoi, A.; Khan, A.A.; Mahto, B.; Bisoyi, A.; Hussain, S. Chelating agent-assisted-Bi2WO6 nanostructured materials for electron transfer-driven ultrafast catalytic reduction of organic and inorganic contaminants. *ChemNanoMat* **2023,** *9,* e202300181. DOI: 10.1002/cnma.202300181
68. Borah, D.; Mishra, V.; Debnath, R.; Ghosh, K.; Gogoi, D.; Rout, J.; Pandey, P.; Ghosh, N.N.; Bhattacharjee, C.R. Facile green synthesis of highly stable, water dispersible carbohydrate conjugated Ag, Au and Ag-Au biocompatible nanoparticles: catalytic and antimicrobial activity. *Mate. Today Commun.* **2023,** *37,* 107096. DOI: 10.1016/j.mtcomm.2023.107096
69. Chabalala, M.B.; Zikalala, S.A.a; Ndlovu, L.; Mamba, G.; Mamba, B.; Nxumalo, E.N. A green synthetic approach for the morphological control of ZnO-Ag using β-cyclodextrin and honey for photocatalytic degradation of bromophenol blue. *Chem. Eng. Res. Des.* **2023,** *197,* 307-322. DOI: 10.1016/j.cherd.2023.07.029
70. Cui, L.; Wen, J.; Deng, Q.; Du, X.; Tang, T.; Li, M.; Xiao, J.; Jiang, L.; Hu, G.; Cao, X.; Yao, Y. Improving the photocatalytic activity of Ti3C2 MXene by surface modification of N doped. *Materials* **2023,** *16,* 2836. DOI: 10.3390/ma16072836
71. Dilawar, S.; Albalawi, K.; Khan, A.U.; Tahir, K.; Zaki, M.E.A.; Musad S.E.A.; Almarhoon, Z.M.; Althagafi, T.M.; El-Zahhar, A.A.; El-Bialy E. Rapid photodegradation of toxic organic compounds and photo inhibition of bacteria in the presence of novel hydrothermally synthesized Ag/Mn–ZnO nanomaterial. *Environ. Res.* **2023,** *231,* 116093. DOI: 10.1016/j.envres.2023.116093
72. Ding, W.; Luo, J.-X.; Gu, Q.; Liu, Z.-H. Ultrathin 2D ZnGa-borate-LDH nanosheets for boosting dye-sensitized photocatalytic coupled reaction of H2 production with pollutant degradation. *Colloids Surf. A Physicochem. Eng. Asp.* **2023,** 657, 130575. DOI: 10.1016/j.colsurfa.2022.130575
73. Dumbrava, A.; Matei, C.; Diacon, A.; Moscalu, F.; Berger, D. Novel ZnO-biochar nanocomposites obtained by hydrothermal method in extracts of *Ulva lactuca* collected from Black Sea. *Ceram. Int.* **2023,** *49,* 10003-10013. DOI: 10.1016/j.ceramint.2022.11.178
74. El Mragui, A.; Aadnan, I.; Zegaoui, O.; Esteves da Silva, J.C.G. Physico-chemical characterization and photocatalytic activity assessment under UV-A and visible-light irradiation of iron-doped TiO2 nanoparticles. *Arabian J. Chem.* **2023,** *16,* 105331. DOI: 10.1016/j.arabjc.2023.105331
75. Franco, R.T.; Silva, A.L.; Licea, Y.E.; Alzamora, M.; Sánchez, D.R.; Carvalho, N.M.F. Effect of *Camellia sinensis* origin and heat treatment in the iron oxides nanomaterials composition and Fenton degradation of methyl orange. *J. Brazilian Chem. Soc.* **2023,** *34,* 694–704. DOI: 10.21577/0103-5053.20220140
76. Hadi, A. Synthesis and characteristics of Y2O3/SiO2/GO hybrid nanoceramics for photo-degradation of organic dyes. *Opt. Quantum Electron.* **2023,** *55,* 551. DOI: 10.1007/s11082-023-04832-7
77. Huang-Mu, L.; Devanesan, S.; Farhat, K.; Kim, W.; Sivarasan, G. Improving the efficiency of metal ions doped Fe_2O_3 nanoparticles: photocatalyst for removal of organic dye from aqueous media. *Chemosphere* **2023,** *337,* 139229. DOI: 10.1016/j.chemosphere.2023.139229
78. Jayaprakash, K.; Sivasamy, A. Polymeric graphitic carbon nitride layers decorated with erbium oxide and enhanced photocatalytic performance under visible light irradiation. *Environ. Sci. Poll. Res.* **2023,** *30,* 52561-52575. DOI: 10.1007/s11356-023-26008-2
79. Khan, Y.; Sharafat, U.; Gul, S.; Khan M.I.; Ismail, M.; Khan, M.A.; Younus, R.; Khan, S.B.. Novel in situ synthesis of quaternary core-shell metallic sulfide nanocomposites for degradation of organic dyes and hydrogen production. *Green Process. Synth.* **2023,** *12,* 20228128. DOI: 10.1515/gps-2022-8128

80. Latif, S.; Abdulaziz, F.; Alanazi, A.M.; Alsehli, A.H.; Alsowayigh, M.M.; Alanazi, A.A. Effect of H_2O_2@CuONPs in the UV light-induced removal of organic pollutant Congo Red dye: investigation into mechanism with additional biomedical study. *Molecules* **2023,** *28,* 410. DOI: 10.3390/molecules28010410
81. Lebière, P.G.; Ivan R.; Pérez del Pino A.; Logofatu C.; Negrila C.; György E. Boron and nitrogen co-doped carbon-based nanomaterials/nickel oxide/hydroxide hybrids for sunlight induced photocatalytic water cleaning. *Colloids Surf. A Physicochem. Eng. Asp.* **2023,** *676,* 132159. DOI: 10.1016/j.colsurfa.2023.132159
82. Liu, S.; Bu, Y.; Cheng, S.; Tao, Y.; Hong, W. Preparation of g-C_3N_5/g-C_3N_4 heterojunction for methyl orange photocatalytic degradation: mechanism analysis. *J. Water Proc. Eng.* **2023,** *54,* 104019. DOI: 10.1016/j.jwpe.2023.104019
83. Ma, A.; Liao, X.; Qian, H.; Liu, J.; Liu, H.; Ren, S. An attapulgite composite with high degradation performance for Congo red without using oxidants and photoexcitation. *Mater. Sci. Eng. B* **2023,** *296,* 116628. DOI: 10.1016/j.mseb.2023.116628
84. Mbarek, W.B.; Al Harbi, M.; Hammami, B.; Khitouni, M.; Escoda, L.; Suñol, J.-J. Nanostructured Mn–Ni powders produced by high-energy ball-milling for water decontamination from RB5 dye. *Crystals* **2023,** *13,* 879. DOI: 10.3390/cryst13060879
85. Medina, M.J.B.; Bueno, J.J.P.; Rodríguez, C.H.; Pérez, A.X.M.; López, M.L.M.; Chacón, J.G.B.; López, C.M.; Robles, M.R.G.; Oza, G. Heterogeneous photocatalysis using electroless deposition of Ni/NiO nanoparticles on silicon nanowires for the degradation of methyl orange. *Curr. Nanosci.* **2023,** *19,* 432–443. DOI: 10.2174/1573413718666220602144340
86. Meteab, M.H.; Hashim, A.; Rabee, B.H. Synthesis and tailoring the morphological, optical, electronic and photodegradation characteristics of PS–PC/MnO_2–SiC quaternary nanostructures. *Opt. Quantum Electron.* **2023,** *55,* 187. DOI: 10.1007/s11082-022-04447-4
87. Monje, D.S.; Mercado, D.F.; Mesa, G.A.P.; Valencia, G.C. Carbon dots decorated magnetite nanocomposite obtained using yerba mate useful for remediation of textile wastewater through a photo-Fenton treatment: *Ilex paraguariensis* as a platform of environmental interest—part 2. *Environ. Sci. Pollution Res.* **2023,** *30,* 3070-3087. DOI: 10.1007/s11356-022-22405-1
88. Nirmal Rajeev, Y.; Maria Magdalane, C.; Hepsibha, S.; Ramalingam, G.; Arjun Kumar, B.; Bhushan Kumar, L.; Sambasivam, S. Europium decorated hierarchical TiO_2 heterojunction nanostructure with enhanced UV light photocatalytic activity for degradation of toxic industrial effluent. *Inorg. Chem. Commun.* **2023,** *157,* 111339. DOI: 10.1016/j.inoche.2023.111339
89. Pandith, A.; Jayaprakash, G.K.; ALOthman, Z.A. Surface-modified CuO nanoparticles for photocatalysis and highly efficient energy storage devices. *Environ. Sci. Pollution Res.* **2023,** *30,* 43320-43330. DOI: 10.1007/s11356-023-25131-4
90. Ramaraj, B.R.; Mahalingam, U.; Ramasamy, P.; Pearce, J.M.; Mayandi, J.; Mahalingam, A. Environmental remediation of real textile dyeing wastewater under visible light and inactivation of pathogenic bacteria using ZnO/CuO nano-needles. *Phys. Status Solidi A* **2023,** *220,* 2200607. DOI: 10.1002/pssa.202200607
91. Sabur, D.A.; Hashim, A.; Habeeb, M.A. Fabrication and exploration the structural and optical properties of Sb_2O_3-GO nanostructures doped PMMA-PC for photodegradation of pollutants dyes. *Opt. Quantum Electron.* **2023,** *55,* 457. DOI: 10.1007/s11082-023-04726-8
92. Sathya Priya B.; Aruchamy, K.; Oh, T.H.; Avula, B.; Hasan, I.; Shanthi M. Synthesis of solar light active reduced graphene oxide-ZnS nanomaterial for photocatalytic degradation and antibacterial applications. *Micromachines* **2023,** *14,* 1324. DOI: 10.3390/mi14071324
93. Shoran, S.; Sharma, A.; Chaudhary, S. Visible light enhanced photocatalytic degradation of organic pollutants with SiO_2/g-C_3N_4 nanocomposite for environmental applications. *Environ. Sci. Pollut. Res.* **2023,** *30,* 98732-98746. DOI: 10.1007/s11356-022-24837-1
94. Singh, A.K.; Giannakoudakis, D.A.; Arkas, M.; Triantafyllidis, K.S.; Nair, Vaishakh. Composites of lignin-based biochar with BiOCl for photocatalytic water treatment: RSM studies for process optimization. *Nanomaterials* **2023,** *13,* 735. DOI: 10.3390/nano13040735
95. Sudhalakshmi J.; Rajathi K. Fabrication of eco-friendly hybrid active imidazole based ionic liquid embedded cadmium oxide-TiO2 catalyst for photoelectrocatalytic and hydrophobic properties. *Asian J. Chem.* **2023,** *35,* 1827-1835. DOI: 10.14233/ajchem.2023.27954

96. Zamani, W.; Rastgar, S.; Hedayati, A. Capability of TiO_2 and Fe_3O_4 nanoparticles loaded onto Algae (Scendesmus sp.) as a novel bio-magnetic photocatalyst to degration of Red195 dye in the sonophotocatalytic treatment process under ultrasonic/UVA irradiation. *Sci. Rep.* **2023,** *13,* 18182. DOI: 10.1038/s41598-023-45274-1
97. Alka; Kumar, S.; Kumari P. Sulfonatocalix[6]arene-decorated magnetite nanomaterials for the removal of organic pollutants from wáter. *Int. J. Environ. Sci. Technol.* **2023,** *20,* 4467-4482. DOI: 10.1007/s13762-022-04145-4
98. Al-Wasidi, A.S.; Khairy, M.; Abdulkhair, B.Y.; Abdelrahman, E.A. Efficient disposal of basic fuchsin dye from aqueous media using $ZrO_2/MgMn_2O_4/Mg(Mg_{0.333}Mn_{1.333})O_4$ as a novel and facilely synthesized nanocomposite. *Inorganics* **2023,** *11,* 363. DOI: 10.3390/inorganics11090363
99. Aziz, T.; Farid, A.; Chinnam, S.; Haq, F.; Kiran, M.; Wani, A.; Alothman, Z.A.; Aljuwayid, A.M.; Habila, M.A.; Akhtar, M.S. Synthesis, characterization and adsorption behavior of modified cellulose nanocrystals towards different cationic dyes. *Chemosphere* **2023,** *321,* 137999. DOI: 10.1016/j.chemosphere.2023.137999
100. El-Aziz, M.E.A.;Youssef A.M.; Kamal, K.H.; Kelnar, I.; Kamel, S. Preparation and performance of bionanocomposites based on grafted chitosan, GO and TiO_2-NPs for removal of lead ions and Basic-red 46. *Carbohydr. Polym.* **2023,** *305,* 120571. DOI: 10.1016/j.carbpol.2023.120571
101. Guo, F.; Guo, S.; Niu, Y.; Qiu, G.; Guo, Y.; Li, Y.; Chen, L.; Zhang, Y.; Wu, J. Efficient removal of methylene blue via two-step modification hazelnut shell biochar: Process intensification, kinetics and thermodynamics. *J. Ind. Eng. Chem.* **2023,** *125,* 105-116. DOI: 10.1016/j.jiec.2023.05.017
102. Hashem, A.A.; Mahmoud, S.A.; Geioushy, R.A.; Fouad, O.A. Adsorption of malachite green dye over synthesized calcium silicate nanopowders from waste materials. *Mater. Sci. Eng. B* **2023,** *295,* 116605. DOI: 10.1016/j.mseb.2023.116605
103. Konopatsky, A.S.; Kalinina, V.V.; Savchenko, A.S.; Leybo, D.V.; Sukhanova, E.V.; Baidyshev, V.S.; Popov, Z.I.; Bondarev, A.V.; Polčák, J.; Shtansky, D.V. Structure, magnetic and adsorption properties of novel FePt/h-BN heteromaterials. *Nano Res.* **2023,** *16,* 1473-1481. DOI: 10.1007/s12274-022-4672-0
104. Lee, H.; Heo, M.H.; Jeong, H.; Kim, S.Y.; Yuk, J.S.; Park, S.H.; Shin, J. Water-redispersible and high-yield α-chitin nanocrystals isolated using electron-beam irradiation as adsorbents to remove heavy metals and dye. *Nanoscale* **2023,** *15,* 10990-11004. DOI: 10.1039/d3nr00760j
105. Nouri, A.; Ang, W.L; Mahmoudi, E.; Chua, S.F.; Mohammad, A.W.; Benamor, A.; Ba-Abbad, M.M.; Leo, C.P. Decoration of polylactic acid on graphene oxide for efficient adsorption of methylene blue and tetracycline. *Chemosphere* **2023,** *322,* 138219. DOI: 10.1016/j.chemosphere.2023.138219
106. Quach, T.P.T.; Doan, L. Surface modifications of superparamagnetic iron oxide nanoparticles with polyvinyl alcohol, chitosan, and graphene oxide as Methylene Blue adsorbents. *Coatings* **2023,** *13,* 1333. DOI: 10.3390/coatings13081333
107. Salahshoori, I.; Jorabchi, M.N.; Ghasemi, S.; Mirnezami, S.M.S.; Nobre, M.A.L.; Khonakdar, H.A. Assessing cationic dye adsorption mechanisms on MIL-53 (Al) nanostructured MOF materials using quantum chemical and molecular simulations: Toward environmentally sustainable wastewater treatment. *J. Water Proc. Eng.* **2023,** *55,* 104081. DOI: 10.1016/j.jwpe.2023.104081
108. Wang, L.; Xue, G.; Ye, T.; Li, J.; Liu, C.; Liu, J.; Ma, P. Zn-modified biochar preparation from solvent free in-situ pyrolysis and its removal of methylene blue. *Diam. Relat. Mater.* **2023,** *140,* 110438. DOI: 10.1016/j.diamond.2023.110438
109. Wang, M.; Jiao, Y.; Li, N.; Su, Y. Synthesis of a SiO_2-MgO composite material derived from yellow phosphorus slag with excellent malachite green adsorption activity. *J. Alloys Comp.* **2023,** *969,* 172344. DOI: 10.1016/j.jallcom.2023.172344
110. Zhu, K.; Mohammed, S.; Tang, H.; Xie, Z.; Fang, S.; Liu, S. ZIF-67/SA@PVDF ultrafiltration membrane with simultaneous adsorption and catalytic oxidation for dyes. *Sustainability* **2023,** *15,* 2879. DOI: 10.3390/su15042879
111. Alenad, A.M.; Waheed, M.S.; Aman, S.; Ahmad, N.; Khan, A.R.; Khosa, R.Y.; Ansari, M.Z.; Khan, S.A.; Farid, H.M.T.; Taha, T.A.M. Visible light driven Ni doped hematite for photocatalytic reduction of noxious methylene blue. *Mater. Res. Bull.* **2023,** *165,* 112306. DOI: 10.1016/j.materresbull.2023.11230 6
112. Algarni, S.A.; Aman, S.; Ahmad, N.; Khan, S.A.; Farid, H.M.T.; Taha, T.A.M. Processing of Nb doped hematite for visible light photocatalytic reduction of noxious methylene blue. *Optik* **2023,** *287,* 171097. DOI: 10.1016/j.ijleo.2023.171097

113. Alizadeh, N.; Salimi, A. Simultaneous adsorption and catalytic degradation of methylene blue dye over recyclable $Mn_4(P_2O_7)3$ nanoflakes: mechanism and efficiency. *Environ. Nanotechnol. Monit. Manag.* **2023,** *20,* 100806. DOI: 10.1016/j.enmm.2023.100806
114. Al-nayili, A.; Khayoon, H.A.; Alshamsi, H.A.; Cata Saady, N.M. A novel bimetallic (Au-Pd)-decorated reduced graphene oxide nanocomposite enhanced Rhodamine B photocatalytic degradation under solar irradiation. *Mater. Today Sust.* **2023,** *24,* 100512. DOI: 10.1016/j.mtsust.2023.100512
115. Bandaru, S.G.; Yathapu, S.; Sathiraju, A.; Ganghishetti, B.; Mangalarapu, T.B.; Singh A.K. Photoluminescence and photocatalytic studies of rice water and papaya fruit extract-encapsulated cadmium sulfide nanoparticles. *J. Korean Ceram. Soc.* **2023,** *60,* 183-202. DOI: 10.1007/s43207-022-00253-6
116. Basfer N.M.; Al-Harbi, N. Structural, optical and photocatalytic activity of Ce^{3+} doped Co–Mg nanoparticles for wastewater treatment applications. *J. King Saud Univ.Sci.* **2023,** *35,* 102436. DOI: 10.1016/j.jksus.2022.102436
117. Bhatti, M.A.; Tahira, A.; Hullio, A.A.; Aftab, U.; Nafady, A.; Vigolo, B.; Ibupoto, Z.H. Oxygenated terminals of milky sap of *Calotropis procera* transformed 1D ZnO structure to 0D nanoparticles for enhanced photocatalytic degradation of malachite green and methylene blue. *J. Mater. Sci. Mater. Electron.* **2023,** *34,* 929. DOI: 10.1007/s10854-023-10290-4
118. Biswakarma, D.; Dey, N.; Bhattacharya, S. Hydrogel nanocomposite towards optical sensing of spermine in biomedical and real-life food samples and remediation of toxic dyes from wastewater. *Langmuir* **2023,** *39,* 11610-11620. DOI: 10.1021/acs.langmuir.3c01128
119. Chellapandi, T.; Roopan, S.M.; Madhumitha, G. Interfacial charge transfer of *Carrisa edulis* fruit extract capped Co_3O4 nanoparticles on the surface of MK30: an efficient photocatalytic removal of methylthioninium chloride and tetracycline organic pollutants. *Environ. Res.* **2023,** *219,* 115052. DOI: 10.1016/j.envres.2022.115052
120. Dang, H.T.M; Nguyen, M.T.T.; Tran, L.T.; Tran, H.V; Huynh, C. Synthesis and photocatalytic activity of a lanthanum doped $CoFe_2O_4/TiO_2$ nanocomposite for photodegradation of methylene blue organic dye. *J. Chem. Res.* **2023,** *47,* 1-7. DOI: 10.1177/17475198221151152
121. Dhiman, P.; Rana, G.; Kumar, A.; Dawi, E.A.; Sharma, G. Rare earth doped ZnO nanoparticles as spintronics and photo catalyst for degradation of pollutants. *Molecules* **2023,** *28,* 2838. DOI: 10.3390/molecules28062838
122. Dinker, M.K.; Raut, S.S.; Kulkarni, P.S. Application of ionic mesoporous silica in selective recovery of tungstate ions through column adsorption and subsequent photocatalytic degradation of an organic dye. *Environ. Sci. Nano* **2023,** *10,* 1883-1896. DOI: 10.1039/d3en00053b
123. Dos Santos, D.F.; Santiago, A.G.; Teodoro, M.D.; Motta, F.V.; Bomio, M.R.D. Investigation of the photocatalytic and optical properties of the $SrMoO_4/g\text{-}C_3N_4$ heterostructure obtained via sonochemical synthesis with temperature control. *J. Environ. Manage.* **2023,** *325,* 116396. DOI: 10.1016/j.jenvman.2022.116396
124. Ehsan, Md.F.; Barai, H.R.; Islam, Md.M.; Susan, Md.A.B.H.; Joo, S.W.; Miran, M.S. ZnO nanocomposites supported by acid-activated kaolinite as photocatalysts for the enhanced photodegradation of an organic dye. *Mater. Today Commun.* **2023,** *36,* 106563. DOI: 10.1016/j.mtcomm.2023.106563
125. El-Shafai, N.M.; Masoud, M.S.; Ramadan, M.S.; El-Mehasseb, I. Engineering design of n/p-type nano heterojunctions loaded on cotton cellulose nanocrystal surface: removal of pollutants and supercapacitors applications. *J. Energy Storage* **2023,** *58,* 106341. DOI: 10.1016/j.est.2022.106341
126. Gadge, A.S.; Janbandhu S.Y.; Sukhadeve, G.K.; Kumar, R.; Gajbhiye, C.D.; Gedam, R.S. TiO_2 nanoparticles for Methylene Blue dye degradation: effect of calcination temperature. *ECS J. Solid State Sci. Technol.* **2023,** *12,* 086004. DOI: 10.1149/2162-8777/acf06f
127. Huang, P.; Fang, W.; Yang, L.; Sun, Y.; Yang, H.; Chen, X.-Z.; Zeng, H. Ultralong hydroxyapatite nanowires-based flow-through reactor with high loading of silver nanoparticles for fast continuous catalytic reduction of organic dyes and disinfection of wastewater. *Chem. Eng. J.* **2023,** *475,* 146305. DOI: 10.1016/j.cej.2023.146305
128. Ivanov, K.V.; Noskov, A.V.; Alekseeva, O.V.; Agafonov, A.V. Effect of annealing conditions on the physicochemical and photocatalytic properties of a nanopowder based on Fe_2TiO_5. *Mater. Chem. Phys.* **2023,** *299,* 127493. DOI: 10.1016/j.matchemphys.2023.127493

129. Jiang, J.; Liang, Y.; Wang, H.; Zhao, J.; Hu, J.; Wang, M. In situ mineralization of akageneite (β-FeOOH) on cotton for water purification via Fenton-like reaction. *Fibers Polym.* **2023,** *24,* 1641-1648. DOI: 10.1007/s12221-023-00154-3
130. Jiang, W.; Xu, Q.; Bu, F.; Wei, Y.; Wang, Y.; Wang, Z.; Jiang, Y. Fabrication of Fe_3O_4@APF magnetic nanospheres with tunable core–shell structure: an effective carrier and reducing agent for Ag nanoparticles. *J. Inorg. Organomet. Polym. Mater.* **2023,** *33,* 2562-2573. DOI: 10.1007/s10904-023-02704-x
131. Karthik, P.; Ravichandran, S.; Sasikala, V.; Prakash, N.; Mukkannan, A.; Rajesh, J. Effective photodegradation of organic water pollutants by the facile synthesis of Ag_2O nanoparticles. *Surf. Interf.* **2023,** *40,* 103088. DOI: 10.1016/j.surfin.2023.103088
132. Kaya, M.T.; Calimli, M.H.; Nas, M.S. Degradation of methylene blue with a novel Fe_3O_4/Mn_3O_4/CuO nanomaterial under sonocatalytic conditions. *Res. Chem. Interm.* **2023,** *49,* 2549-2568. DOI: 10.1007/s11164-023-04964-1
133. Ma, A.; Qian, H.; Liu, H.; Ren, S. Degradation of malachite green by g-C_3N_4-modified magnetic attapulgite composites under visible-light conditions. *Environ. Sci. Pollution Res.* **2023,** *30,* 96360-96375. DOI: 10.1007/s11356-023-29201-5
134. Ma, D.; Pan, S.; Tan, M.; He, G.; Zhao, J. Shape-controlled synthesis of varied bismuth nanostructures and their size-dependent photocatalytic removal of organic dyes under visible light irradiation. *Opt. Mater.* **2023,** *145,* 114433. DOI: 10.1016/j.optmat.2023.114433
135. Magomedova, A.; Isaev, A.; Orudzhev, F.; Alikhanov, N.; Emirov, R.; Rabadanov, M.; Mingshan, Z. Electrochemical synthesis of superparamagnetic Fe_3O_4 nanoparticles for the photo-Fenton oxidation of Rhodamine B. *ChemistrySelect* **2023,** *8,* e202301694. DOI: 10.1002/slct.202301694
136. Malathy A.; Manikandan V.; Devanesan, S.; Farhat, K.; Priyadharsan A.; Ragavendran C.; Ragupathy S.; Ranjith R.; Sivakumar S. Development of biohybrid Ag_2CrO_4/rGO based nanocomposites with stable flotation properties as enhanced photocatalyst for sewage treatment and antibiotic-conjugated for antibacterial evaluation. *Int. J. Biol. Macromol.* **2023,** *244,* 125303. DOI: 10.1016/j.ijbiomac.2023.125303
137. Maru, M.T.; Gonfa, B.A.; Zelekew, O.A.; Fakrudeen, S.P.; Ananda Murthy H.C.; Bekele, E.T.; Sabir, F.K. Effect of Musa acuminata peel extract on synthesis of ZnO/CuO nanocomposites for photocatalytic degradation of methylene blue. *Green Chem. Lett. Rev.* **2023,** *16,* 2232383. DOI: 10.1080/17518253.2023.2232383
138. Munusamy S.; Venkatesan, Raja; Divya S.; Gnanamoorthy G.; Narayanan V.; Vivekananthan, V.; Ansar, S.; Oh, T.-H.; Kim, S.-C. Electrochemical and photochemical characteristics of organic dyes and biological molecules at conducting polymer-modified electrodes of indium oxide-polypyrrole nanohybrids. *Mater. Sci. Eng. B* **2023,** *297,* 116761. DOI: 10.1016/j.mseb.2023.116761
139. Negem, M.; Miller, D.; Irvine, J.; Heakal, F.E.-T. Water/oil nanoemulsion-based synthesis of $Bi_xSn_{6-2x}S_y$ ($0.33 \leq x \leq 2.95$) semiconductor QDs for efficient photocatalytic degradation of MB dye. *Environ. Sci. Poll. Res.* **2023,** *30,* 58998-59012. DOI: 10.1007/s11356-023-26596-z
140. Perumal V.; Uthrakumar R.; Chinnathambi M.; Inmozhi C.; Robert R.; Rajasaravanan M.E.; Raja A.; Kaviyarasu K. Electron-hole recombination effect of SnO_2–CuO nanocomposite for improving methylene blue photocatalytic activity in wastewater treatment under visible light. *J. King Saud Univ. Sci.* **2023,** *35,* 102388. DOI: 10.1016/j.jksus.2022.102388
141. Raveendran Nair, P.; Rosa Santiago Ramirez, C.; Angel Gracia Pinilla, M.; Krishnan, B.; Avellaneda Avellaneda, D.; Fabian Cienfuegos Pelaes, R. Black titanium dioxide nanocolloids by laser irradiation in liquids for visible light photo-catalytic/electrochemical applications. *Appl. Surf. Sci.* **2023,** *623,* 157096. DOI: 10.1016/j.apsusc.2023.157096
142. Saeed, M.; Pecho, R.D.C.; Panchal, S.; Alhag, S.K.; Al-Shuraym, L.A.; Al Syaad, K.M.; Bhutta, U.H. Synthesis of Ag-OMS catalyst for sunlight-assisted photodegradation of Crystal Violet dye. *Water* **2023,** *15,* 2480. DOI: 10.3390/w15132480
143. Saif, N.; Tariq, A.; Intisar, A.; Batool, Z.; Arshad, M.; ur Rehman, A.; Kousar, R. Green synthesis of SnO_2 nanorods and Mo–SnO_2 nanocomposite for efficient sunlight driven organic dye photodegradation in aqueous solution. *Mater. Chem. Phys.* **2023,** *305,* 127920. DOI: 10.1016/j.matchemphys.2023.127920
144. Sasikala, V.; Karthik, P.; Ravichandran, S.; Prakash, N.; Rajesh, J.; Mukkannan, A. Effective removal of organic dyes using novel $MnWO_4$ incorporated CA/PCL nanocomposite membranes. *Surf. Interf.* **2023,** *40,* 103008. DOI: 10.1016/j.surfin.2023.103008

 doi:10.20944/preprints202405.1122.v1

145. Selvaraj, S.; Natesan, K.; Bhargav, P. B.; Nafis A. Revolutionizing water treatment: Exploring the efficacy of MoS_2/BN/rGO ternary nanocomposite in organic dye treated water for OER and HER applications. *J. Water Proc. Eng.* **2023,** *54,* 104033. DOI: 10.1016/j.jwpe.2023.104033
146. Sepúlveda, M.; Saldan, I.; Mahnaz, A.; Cicmancova, V.; Michalicka, J.; Hromadko, L.; Bulánek, R.; Sopha, H.; Macak, J.M. Magnetically guidable single TiO_2 nanotube photocatalyst: Structure and photocatalytic properties. *Ceram. Int.* **2023,** *49,* 6764-6771. DOI: 10.1016/j.ceramint.2022.10.197
147. Sewnet, A.; Alemayehu, E.; Abebe, M.; Mani, D.; Thomas, S.; Kalarikkal, N.; Lennartz, B. Single-step synthesis of graphitic carbon nitride nanomaterials by directly calcining the mixture of urea and thiourea: application for Rhodamine B (RhB) dye degradation. *Nanomaterials* **2023,** *13,* 762. DOI: 10.3390/nano13040762
148. Shahanas, T.; Harichandran, G. PEG mediated $NiMn_2O_4$ nanomaterials as a nano catalyst for peroxidase mimetic activity and photocatalytic degradation. *Spectrochim. Acta A Mol. Biomol. Spectrosc.* **2023,** *303,* 123212. DOI: 10.1016/j.saa.2023.123212
149. Soltani, S.; Gacem, A.; Choudhary, N.; Yadav, V.K.; Alsaeedi, H.; Modi, S.; Patel, A.; Khan, S.H.; Cabral-Pinto, M.M.S.; Yadav, K.K.; Patel, A. Scallion peel mediated synthesis of zinc oxide nanoparticles and their applications as nano fertilizer and photocatalyst for removal of organic pollutants from wastewater. *Water* **2023,** *15,* 1672. DOI: 10.3390/w15091672
150. Suganthi, S.; Vignesh, S.; Raj, V.; Manoharadas, S.; Pandiaraj, S.; Kim, H. Synergistic influence of vanadium pentoxide-coupled graphitic carbon nitride composite for photocatalytic degradation of organic pollutant: Stability and involved Z-scheme mechanism. *Environ. Res.* **2023,** *231,* 116288. DOI: 10.1016/j.envres.2023.116288
151. Sukhadeve, G.K.; Gedam, R.S. Visible light assisted photocatalytic degradation of mixture of reactive ternary dye solution by Zn–Fe co-doped TiO_2 nanoparticles. *Chemosphere* **2023,** *341,* 139990. DOI: 10.1016/j.chemosphere.2023.139990
152. Syed, N.; Feng, Y.; Fahad, R.; Huang, J.; Mahar, F.K. Carbon-based composite nanofibers for photocatalytic degradation of methylene blue dye under visible light. *Polym. Adv. Technol.* **2023,** *34,* 2286-2297. DOI: 10.1002/pat.6049
153. Tahir, M.Y.; Sillanpaa, M.; Almutairi, T.M.; Mohammed, A.A.A.; Ali, S. Excellent photocatalytic and antibacterial activities of bio-activated carbon decorated magnesium oxide nanoparticles. *Chemosphere* **2023,** *312,* 137327. DOI: 10.1016/j.chemosphere.2022.137327
154. Thambidurai R.;Gobi G.; Chandrasekar M.; Uthrakumar R.; Inmozhi C.; Kaviyarasu K. ZnO nanocomposites containing Cd are synthesized with high photodegradation potential for wastewater treatment. *J. King Saud Univ. Sci.* **2023,** *35,* 102915. DOI: 10.1016/j.jksus.2023.102915
155. Thambidurai R.; Gobi G.; Uthrakumar R.; Inmozhi C.; Kaviyarasu K. Characterizations of MnO_2 doped TiO_2 nanostructures and effective degradation of methylene blue dye under visible light irradiation. *Dig. J. Nanomater. Biostructures* **2023,** *18,* 869-879. DOI: 10.15251/DJNB.2023.183.869
156. Venkatesan D.; Umasankar S.; Mangesh V.L.; Krishnan, P.. Tamizhdurai P.; Kumaran R.; Baskaralingam P. Removal of Toluidine blue in water using green synthesized nanomaterials. *South African J. Chem. Eng.* **2023,** *45,* 42-50. DOI: 10.1016/j.sajce.2023.04.006
157. Wang, Q.; Lu, J.; Yu, M.; Li, H.; Lin, X.; Nie, J.; Lan, N.; Wang, Z. Sulfur vacancy rich MoS_2/$FeMoO_4$ composites derived from MIL-53(Fe) as PMS activator for efficient elimination of dye: nonradical $^1O_2$ dominated mechanism. *Environ. Pollut.* **2023,** *333,* 121990. DOI: 10.1016/j.envpol.2023.121990
158. Wu, H.; Yang, Q.; Wang, J.; Zhou, H.; Qin, S.; Pan, J.; Li, C. Preparation of CuO nanosheet array thin film with controlled morphology for SERS and photocatalysis. New J. Chem. **2023,** *47,* 6602-6611. DOI: 10.1039/d2nj06073f
159. Yang, M.; Jin, H.; Gui, R. Ag+-doped boron quantum dots with enhanced stability and fluorescence enabling versatile practicality in visual detection, sensing, imaging and photocatalytic degradation. *J. Coll. Interf. Sci.* **2023,** *639,* 49-58. DOI: 10.1016/j.jcis.2023.02.066
160. Zhang, Q.; Wang, D.; Yu, R.; Luo, L.; Li,W.; Cheng, J.; Zhang, Y. Excellent photocatalytic degradation of rhodamine B over Bi_2O_3supported on Zn-MOF nanocomposites under visible light. *Green Proc. Synth.* **2023,** *12,* 20228123. DOI: 10.1515/gps-2022-8123
161. Zhao, W.K.; Ma, Z.Q.; Zheng, J.Y.; Han, C.B.; Zhou, K.L.; Hao, M.Y.; Fang, D.C.; Xia, Y.; Yan, H. Dual-functional MnS_2/MnO_2 heterostructure catalyst for efficient acidic hydrogen evolution reaction and assisted degradation of organic wastewater. *J. Energy Chem.* **2023,** *87,* 215-224. DOI: 10.1016/j.jechem.2023.08.004

162. Zheng, J.Y.; He, J.; Han, C.B.; Huang, G.; Sun, B.C.; Zhao, W.K.; Wang, Y.; Sun, L.; Si, J.; Yan, H. Adsorption-enhanced catalytic oxidation for long-lasting dynamic degradation of organic dyes by porous manganese-based biopolymeric catalyst. *Int. J. Biol. Macromol.* **2023,** *237,* 124152. DOI: 10.1016/j.ijbiomac.2023.124152
163. Basta, A.H.; Lotfy, V.F. Sustainable development of pulping by-product for limiting its pollution risk and production new aerogel-based carbon nanostructures for dyes adsorption. *J. Clean. Prod.* **2023,** *428,* 139275. DOI: 10.1016/j.jclepro.2023.139275
164. Hua, Z.; Tang, L.; Wu, M.; Fu, J. Graphene hydrogel improves *S. putrefaciens*' biological treatment of dye wastewater: Impacts of extracellular electron transfer and function of c-type cytochromes. *Environ. Res.* **2023,** *236,* 116739. DOI: 10.1016/j.envres.2023.116739
165. Li, X.-Y.; Wang, W.-R.; Xue, R.-C.; Chen, P.-Y.; Wang, Y.; Yu, L.-P. Carbon dots/silica nanoaggregates for highly efficient adsorption of alizarin red S and malachite green dyes. *New J. Chem.* **2023,** *47,* 8965-8973. DOI: 10.1039/d3nj01273e
166. Oviedo, L.R.; Oviedo, V.R.; Dalla Nora, L.D.; da Silva, W.L. Adsorption of organic dyes onto nanozeolites: A machine learning study. *Sep. Purif. Technol.* **2023,** *315,* 123712. DOI: 10.1016/j.seppur.2023.123712
167. Poornachandhra, C.; Jayabalakrishnan, R.M.; Balasubramanian, G.; Lakshmanan, A.; Selvakumar S.; Maheswari, M.; John, J.E. Coconut husk fiber: a low-cost bioresource for the synthesis of high-value nanocellulose. *Biointerface Res. Appl. Chem.* **2023,** *13,* 504. DOI: 10.33263/BRIAC136.504
168. Sharma, A.; Mittal, R.; Sharma, P.; Pal, K.; Mona, S. Sustainable approach for adsorptive removal of cationic and anionic dyes by titanium oxide nanoparticles synthesized biogenically using algal extract of *Spirulina*. *Nanotechnology* 2023, 34, 485301. DOI: 10.1088/1361-6528/acf37e
169. Kallem, P.; Elashwah, N.; Bharath, G.; Hegab, H.M.; Hasan, S.W.; Banat, F. Zwitterion-grafted 2D MXene (Ti3C2TX) nanocomposite membranes with improved water permeability and self-cleaning properties. *ACS Appl. Nano Mater.* **2023,** *6,* 607-621. DOI: 10.1021/acsanm.2c04722
170. Lim, J.H.X.; Goh, K.; Ng, D.Y.F.; Chew, J.; Wang, R. Layer-by-layer hierarchically structured nanofibrous membrane scaffolds incorporating metal-organic framework and carbon nanotube adsorbents for high-performance versatile organic solvent recovery. *J. Clean. Prod.* **2023,** *404,* 136925. DOI: 10.1016/j.jclepro.2023.136925
171. Natesan, G.; Rajappan, K. GO–CuO nanocomposites assimilated into CA–PES polymer membrane in adsorptive removal of organic dyes from wastewater. *Environ. Sci. Poll. Res.* **2023,** *30,* 42658-42678. DOI: 10.1007/s11356-022-21821-7
172. Zhao, D.L.; Jin, H.; Zhao, Q.; Xu, Y.; Shen, L.; Lin, H.; Chung, T.-S. Smart integration of MOFs and CQDs to fabricate defect-free and self-cleaning TFN membranes for dye removal. *J. Membr. Sci.* **2023,** *679,* 121706. DOI: 10.1016/j.memsci.2023.121706
173. Aadil, M.; Kousar, T.; Hussain, M.; Somaily H.H.; Abdulla, A.K.; Muhammad, E.R.; Al-Abbad, E.A.; Salam, M.A.; Albukhari, S.M.; Baamer, D.F.; Ansari, M.Z. Generation of mesoporous n-p-n (ZnO–CuO–CeO_2) heterojunction for highly efficient photodegradation of micro-organic pollutants. *Ceram. Int.* **2023,** *49,* 4846-48541. DOI: 10.1016/j.ceramint.2022.09.375
174. Ahmad, I.; Safdar, M.; Yasmin, N.; Iftikhar, A.; Kalsoom, A.; Khalid, S.; Shams, Z.E.; Mirza, M. Rare earth ions (La^{3+},Nd^{3+}) substituted cobalt–strontium spinel ferrites for photocatalytic degradation of textile dyes. *Water Pract. Technol.* **2023,** *18,* 1742-1755. DOI: 10.2166/wpt.2023.119
175. Alp, E.; Borazan, İ. The production of highly efficient visible-light-driven electrospun α-Fe_2O_3 photocatalyst through modifying iron source material for wastewater treatment applications. *J. Chinese Chem. Soc.* **2023,** *70,* 1510-1520. DOI: 10.1002/jccs.202300157
176. Bibi, S.; Shah, S.S.; Muhammad, F.; Siddiq, M.; Kiran, L.; Aldossari, S.A.; Sheikh Salek Mushab, M.; Sarwar, S. Cu-doped mesoporous TiO_2 photocatalyst for efficient degradation of organic dye via visible light photocatalysis. *Chemosphere* **2023,** *339,* 139583. DOI: 10.1016/j.chemosphere.2023.139583
177. Desseigne, M.; Chevallier, V.; Madigou, V.; Coulet, M.-V.; Heintz, O.; Ait Ahsaine, H.; Arab, M. Plasmonic photocatalysts based on Au nanoparticles and WO_3 for visible light-induced photocatalytic activity. *Catalysts* **2023,** *13,* 1333. DOI: 10.3390/catal13101333
178. Devendrapandi, G.; Padmanaban, D.; Thanikasalam, R.; Panneerselvam, A.; Palraj, R.; Rajabathar, J.R.; Rajendiran, N.; Balu, R.; Oh, T.H.; Ramasundaram, S. Direct sunlight induced room temperature synthesis of anticancer and catalytic silver nanoparticles by shrimp shell waste derived chitosan. *Int. J. Biol. Macromol.* **2023,** *252,* 126205. DOI: 10.1016/j.ijbiomac.2023.126205

179. Elumalai, G.; Maruthai, J.; Jayaraman, K.; Ramachandran, K.; Mathiyalagan, K. *Basella alba* leaves-assisted eco-fabrication of Ag/ZnO nanocomposites for anti-bactericidal activity and catalytic degradation of anthropogenic pollutants. *Chem. Eng. Technol.* **2023,** *46,* 363-372. DOI: 10.1002/ceat.202200311
180. Koca, F.D.; Muhy, H.M.; Halici, M.G. Synthesis of hybrid Cu nanoflowers by using *Tornabea scutellifera* lichen extract, and evaluation of their dye degredation, and antioxidant activities. *S. Afr. J. Bot.* **2023,** *160,* 394-401. DOI: 10.1016/j.sajb.2023.07.036
181. Kumar, A.; Rawat, R.K.; Chauhan, P. Hierarchical α-MoO_3: A versatile eco-friendly material for humidity-assisted ammonia sensing and efficient catalytic activity in wastewater treatment. *Colloids Surf. A Physicochem. Eng. Asp.* **2023,** *676,* 132147. DOI: 10.1016/j.colsurfa.2023.132147
182. Lei, H.; Cui, X.; Jia, X.; Qi, J.; Wang, Z.; Chen, W. Enhanced tribocatalytic degradation of organic pollutants by ZnO nanoparticles of high crystallinity. *Nanomaterials* **2023,** *13,* 46. DOI: 10.3390/nano13010046
183. Long, L.; Xu, K.; Bing Tan, K.; Cai, D.; Yang, Y.; Zhou, S.-F.; Zhan, G. Highly active Mn-Cu bimetallic oxide catalyst assembled as 3D-printed monolithic agitating paddles for advanced oxidation process. *Chem. Eng. Sci.* **2023,** *266,* 118278. DOI: 10.1016/j.ces.2022.118278
184. Lu, Y.; Qin, X.; Hong, J. Synergistic effects of multiple heterojunctions and dopant atom for enhancing the photocatalytic activity of C-modified Zn-doped TiO_2 nanofiber film. *Coatings* **2023,** *13,* 647. DOI: 10.3390/coatings13030647
185. Mansur, A.A.P.; Custódio, D.A.C.; Dorneles, E.M.S.; Coura, F.M.; Carvalho, I.C.; Lage, A.P.; Mansur, H.S. Nanoplexes of ZnS quantum dot-poly-L-lysine/iron oxide nanoparticle-carboxymethylcellulose for photocatalytic degradation of dyes and antibacterial activity in wastewater treatment. *Int. J. Biol. Macromol.* **2023,** *231,* 123363. DOI: 10.1016/j.ijbiomac.2023.123363
186. Maro, C.A.G.; Gálvez, H.E.G.; Olivas, O.J.N.; Morales, M.L.; Hernández, D.V.; Flores, H.G.; Carmona, V.M.O.; Chinchillas, M.J.C. Peumus boldus used in the synthesis of ZnO semiconductor nanoparticles and their evaluation in organic contaminants. *Materials* **2023,** *16,* 4344. DOI: 10.3390/ma16124344
187. Najafidoust, A.; Haghighi, M.; Abbasi Asl, E.; Bananifard, H. Sono-precipitation dispersion of CuO-doped ZnO nanostructures over SiO_2-aerogel for photo-removal of methylene blue, congo red and methyl orange from wastewater. *J. Ind. Eng. Chem.* **2023.** DOI: 10.1016/j.jiec.2023.10.036
188. Nascimento Júnior, W.J.; de Aguiar, G.H.; Landers, R.; Vieira, M.G.A.; Motta Sobrinho, M.A. Potential of the main magnetic iron oxides synthesized over graphene oxide in integrated adsorption and photocatalysis of inorganic and organic emergent contaminants. *Colloids Surf. A Physicochem. Eng. Asp.* **2023,** *671,* 131647. DOI: 10.1016/j.colsurfa.2023.131647
189. Nayak, R.R.; Gupta, T.; Chauhan, R.P. Organic waste peel–assisted synthesis of ZnSe nanoparticles for solar-driven photocatalytic degradation of cationic and anionic dye. *Environ. Sci. Pollut. Res.* **2023,** *30,* 88167-88179. DOI: 10.1007/s11356-023-28630-6
190. Özcan, S.; Süngü Akdoğan, Ç.Z.; Polat, M.; Kip, Ç.; Tuncel, A. A new multimodal magnetic nanozyme and a reusable peroxymonosulfate oxidation catalyst: manganese oxide coated-monodisperse-porous and magnetic core-shell microspheres. *Chemosphere* **2023,** *341,* 140034. DOI: 10.1016/j.chemosphere.2023.140034
191. Rahmatian, N.; Abbasi, S.; Tavakkoli Yaraki, M.; Abbasi, N. *Echinophora platyloba* extract-mediated green synthesis of silver nanoparticles: Fine-tuning the size towards enhanced catalytic and antibacterial properties. *J. Mol. Liq.* **2023,** *391,* 123327. DOI: 10.1016/j.molliq.2023.123327
192. Rani M.; Keshu; Shanker U. Efficient visible light photocatalytic organic colorants elimination performance induced by biosynthesized titanium dioxide coupled cadmium sulfide nanostructures. *Int. J. Environ. Sci. Technol.* **2023,** *20,* 5491-5508. DOI: 10.1007/s13762-022-04255-z
193. Safo, K.; Noby, H.; Mitsuhara, M.; Naragino, H.; El-Shazly, A.H. H_2O_2 assisted steel slag nanocomposite for degradation of organic pollutant in an advanced oxidation process for suspension and Spin-Coated mode. *Environ. Nanotechnol. Monit. Manag.* **2023,** *20,* 100836. DOI: 10.1016/j.enmm.2023.100836
194. Shaik, M.R.; Aldhuwayhi, F.N.; Al-Mohaimeed, A.M.; Hatshan, M.R.; Kuniyil, M.; Adil, S.F.; Khan, M. Morphology controlled deposition of vanadium oxide (VO_x) nanoparticles on the surface of highly reduced graphene oxide for the photocatalytic degradation of hazardous organic dyes. *Materials* **2023,** *16,* 6340. DOI: 10.3390/ma16186340
195. Song, C.-L.; Li, Z.; Zhang, Y.-N.; Zhang, G.; Yang, Y.-W. Hydrazide–pillar[5]arene-mediated silver nanoparticles for highly efficient reductive degradation of organic dyes. *Supramol. Mater.* **2023,** *2,* 100035. DOI: 10.1016/j.supmat.2023.100035

196. Torres-Torres, K.; Nash-Montes, V.I.; Luciano-Velázquez, J.; Bailón-Ruiz, S.J. Photocatalysis degradation of Remazol Brilliant Blue R and Brilliant Green by zinc-based nanomaterials. *MRS Adv.* **2023,** *8,* 392-396. DOI: 10.1557/s43580-022-00374-4
197. Stanley, R.; Balu, S.K.; Alphas J.J.; Manisha Vidyavathy, S. Super-efficient photocatalytic degradation of methylene blue, methyl orange and rhodamine B dyes using low-cost ZnO–MgO nanocomposite under natural sunlight and its bactericidal activity. *Res. Chem. Intermed.* **2023,** *49,* 2583-2602. DOI: 10.1007/s11164-023-04985-w
198. Yadav, S.; Rani, N.; Saini, K. Coupling ZnO with CuO for efficient organic pollutant removal. *Environ. Sci. Poll. Res.* **2023,** *30,* 71984-72008. DOI: 10.1007/s11356-022-24139-6
199. Yousefi, F.; Haghighi, M.; Shabani, M. Potato-on-rod like of Z-scheme plasmon Ag_2CrO_4-$Ag_2Mo_2O_7$ heterojunction nanophotocatalyst with high stability and accelerated photo-degradation evolution of organic contaminants. *Environ. Res.* **2023,** *236,* 116853. DOI: 10.1016/j.envres.2023.116853
200. Zhao, S.-Z.; Yang, Y.; Lu, R.; Wang, Y.; Huang, H.-L.; Hu, Y.-D.; Rodriguez, R.D.; Chen, J.-J. Bi_2O_3/$Bi_2O_{2.33}$@ECNF: A recyclable material for efficient adsorption and photocatalytic degradation of organic contaminants. *Colloids Surf. A Physicochem. Eng. Asp.* **2023,** *674,* 131912. DOI: 10.1016/j.colsurfa.2023.131912